A full year of continuous net soil and ditch CO_2, CH_4, N_2O fluxes, soil hydrology and meteorology for a drained fen in Denmark

Annelie S. Nielsen[1], Klaus S. Larsen[1], Poul Erik Lærke[2], Andres F. Rodriguez[2], Johannes W. M. Pullens[2], Rasmus J. Petersen[3], and Jesper R. Christiansen[1]

[1]Department of Geoscience and Natural Resource Management, University of Copenhagen, Frederiksberg, 1958, Denmark
[2]Department of Agroecology, Aarhus University, Tjele, 8830, Denmark
[3]Department of Ecoscience, Aarhus University, Aarhus, 8000, Denmark

Correspondence: Jesper R. Christiansen (jrc@ign.ku.dk)

Abstract. We present a detailed dataset (https://doi.org/10.60612/DATADK/BZQ8JE, Skov Nielsen et al., 2025) of automated greenhouse gas (GHG) net soil and ditch fluxes of carbon dioxide (CO_2), methane (CH_4), and nitrous oxide (N_2O) from a drained fen in Denmark covering a full year. The dataset resolves small scale spatial and hourly-daily-seasonal dynamics of GHG soil fluxes. The GHG flux dataset is accompanied by simultaneous time series of soil temperature and moisture, as well as groundwater table depth and covers spatiotemporal gradients in soil hydrological and climatic variability. The GHG fluxes of CO_2, CH_4 and N_2O were measured simultaneously by a high-precision cavity ring down laser spectrometer connected with a novel automated GHG system platform called SkyLine2D (Earthbound Scientific Ltd., UK) that allowed up to 27 individual chamber measurement points along a 24 m transect. In total 47.483 chamber measurements were completed and after quality control 44.631 CO_2 fluxes, 44.099 N_2O and 42.515 CH_4 fluxes remained.

The average ($\pm$SE) net soil CO_2 efflux observed at the site ($2.6 \pm 0.02\ \mu mol\ CO_2\ m^{-2}\ s^{-1}$ or $35 \pm 0.3\ tCO_2\ ha^{-1}\ yr^{-1}$) aligns with findings from similar drained fens in northern Europe covering substantial spatial variability. The organic soil at the site was a larger net source of N_2O ($8.9 \pm 0.1\ nmol\ N_2O\ m^{-2}\ s^{-1}$ or $123 \pm 1.4\ kg\ N_2O\ ha^{-1}\ yr^{-1}$) to the atmosphere compared to other temperate drained organic grassland soils in northern Europe with similar spatial variability as soil CO_2 effluxes. However, the temporal variability of N_2O fluxes were closely linked to fluctuations of the groundwater table depth with emission bursts of soil N_2O emissions during low water table depth. N_2O fluxes decreased to near-zero fluxes when the water table depth increased. Net soil CH_4 fluxes were near-zero and the site overall acted as a smaller net source ($0.18 \pm 0.06\ nmol\ CH_4\ m^{-2}\ s^{-1}$ or $0.91 \pm 0.3\ kg\ CH_4\ ha^{-1}\ yr^{-1}$) compared to other drained organic grassland soils, although net uptake of atmospheric CH_4 was observed as well especially in drier conditions. Compared to the peat soil, the ditch was a smaller net source of CO_2 ($0.94 \pm 0.05\ \mu mol\ CO_2\ m^{-2}\ s^{-1}$ or $1.3 \pm 0.7\ tCO_2\ ha^{-1}\ yr^{-1}$) and N_2O ($0.35 \pm 0.03\ nmol\ N_2O\ m^{-2}\ s^{-1}$ or $4.9 \pm 0.4\ kg\ N_2O\ ha^{-1}\ yr^{-1}$). The ditch emission of CH_4 ($161 \pm 13\ nmol\ CH_4\ m^{-2}\ s^{-1}$ or $812 \pm 66\ kg\ CH_4\ ha^{-1}\ yr^{-1}$) average of diffusive and ebullition fluxes) to the atmosphere was more than two orders of magnitude larger than the net soil CH_4 emissions.

The very large number of fluxes of CO_2, N_2O and CH_4 for peat soils and a ditch linked to both groundwater table data, soil moisture/temperature as well as groundwater and soil physicochemical parameters are unique to northern temperate peatlands and holds a potential for exploring and testing basic hypothesis on the simultaneous regulation of these gas fluxes by both soil hydrology and temperature, including soil and groundwater chemistry. The high temporal detail also allows for time series analyses as well as investigations into diurnal and seasonal patterns of fluxes in response to physical drivers. Similarly, the high frequency of measured variables and the

large number of spatial replicates are furthermore well suited for testing biogeochemical models as it is possible to have both calibration and validation dataset covering the same period. Furthermore, the surprisingly large spatial variability of flux data is ideal to include in model sensitivity tests which can aid in constraining model outputs and develop model routines.

1 Introduction

Understanding the climate feedback of temperate drained and rewetted wetlands requires robust observational datasets of net fluxes, e.g. whether the rewetted peatlands act as net sources to the atmosphere or sinks of greenhouse gases (GHG). This necessitates being able to capture spatial and temporal variability from these systems. Flux data covering all three major GHGs are rare for temperate peatlands, and despite growing efforts to quantify GHG fluxes from drained peatlands, existing datasets often suffer from limited temporal resolution, short monitoring periods, or a lack of concurrent hydrological and meteorological data. Many studies rely on manual chamber-based campaigns that may be able to capture overall seasonal dynamics, but fail to capture short term transient emission phenomenon in response to fluctuations in physical drivers, for example fluctuating groundwater. Also, manual based measurements are labour intensive limiting the number of spatial replicates. Moreover, current high temporal resolution datasets for wetlands using eddy covariance typically offer high good quality for a specific wetland site, but it is challenging to derive the specific spatial variability across the different sub-environments within the wetland, for example between hummocks and hollows with different GHG emission profiles. This discrepancy between spatial and temporal coverage of current flux methodologies in wetlands in turn hampers the ability to develop precise models that integrate spatiotemporal patterns and can forecast GHG fluxes at the ecosystem scale more precisely. This can impact the ability to predict climatic feedback of wetlands now and under future alteration of these systems driven by land use and climatic changes.

However, automated GHG closed chamber flux measurements from ecosystems are becoming increasingly common, also in peatland research (Anthony and Silver, 2023; Boonman et al., 2024) as equipment costs decrease and awareness grows about the importance of resolving temporal variability of GHG fluxes to better understand soil biogeochemical processes and soil-climate feedback. But high-frequency data of GHG fluxes are still scarce for peatlands and spatial variability of fluxes is rarely represented as well due to limited number of spatial replicates. Thus, most automated chamber systems are setup around a multiplexer control unit linking multiple chambers with one or more GHG analysers. State-of-the-art automatic chamber systems, like the LI-8250 Automated Gas Flux System (LiCOR, USA) or the eosAC-LT/LO (Eosense Inc. Canada), i.e. allow for a standard number of 8 or 16 chambers, respectively, that can be upgraded to 36 chambers with additional manifolds. Such large replicate chambers allow for improved characterization of spatial variation or treatment effects coupled with temporal variations but are costly to establish.

We here present a dataset that addresses the abovementioned limitations by combining high-frequency, continuous measurements of net soil fluxes of carbon dioxide (CO_2), methane (CH_4) and nitrous oxide (N_2O) with detailed hydrological and meteorological variables. The GHG fluxes were measured with an automated GHG chamber system, called SkyLine2D, over 12 months resolving spatiotemporal patterns of GHG fluxes including 27 individual collars (26 on organic soil and 1 in a ditch) over a 24 m transect on a temperate drained fen peatland. Integrated quality control, flagging of erroneous or uncertain flux measurements enabled objective filtering of poor-quality data on the entire dataset. This comprehensive spatiotemporal coverage enables robust calibration and validation of biogeochemical and hydrological models, particularly those aiming to simulate the complex interactions between water table dynamics, soil processes, and GHG emissions in managed peatland systems.

Considering the critical need for obtaining high-quality data on soil GHG fluxes from natural and restored peatlands in Europe and globally, our dataset marks an important contribution to this endeavour as it addresses current data shortcomings for Danish and European peatlands by providing detailed data on temporal and spatial patterns of GHG fluxes from organic soils and drainage ditches together with environmental drivers of soil hydrology and temperature, organic soil properties and groundwater geochemistry. We publish this data with the aim of it being used by the scientific community for both experimentalists to test hypothesis of how GHG dynamics are related to hydrology, soil, geochemistry and climate, as well as for the modelers to test and develop biogeochemical models for peatlands.

2 Materials and Methods

2.1 Site description

The field site, Vejrumbro (N 56.43819 E 9.54527 (WGS 84)), is located in Central Jutland, in Denmark near the city of Viborg (Fig. 1A) with a mean annual temperature of 8.3 °C and annual precipitation of 675 mm for the period 1991–2020 (measured 6 km away at Aarhus University Viborg Meteorological Station in Foulum, Jørgensen et al., 2023). It is sit-

uated in the Nørre Å valley and is characterized as a riparian fen peat soil (Reza Mashhadi et al., 2024). The riparian fen developed in a former glacial river valley with flat topography gently sloping (< 2.5 m over 300 m) towards the Nørre Å that forms the central river in this area (Fig. S1 in the Supplement). The site was drained in 1950 with ditches and tile drains for cultivation and was used to cut hay for fodder as the conditions were unfavourable for cereal production (Nielsen et al., 2024). Since 2018, Vejrumbro has been a living lab for agroecological research managed by the Department of Agroecology at Aarhus University. From 2018, the site had a passive rewetting strategy by terminating maintenance of the open ditches. During 2022, the main ditches were gradually blocked.

2.1.1 Site preparation

We chose to perform the flux measurements without aboveground plants as the small chamber dimensions (height of 20 cm) prohibited inclusion of these in the chamber as the plants typically reach over 100 cm in height at this site. The strategy was therefore to focus on measuring net soil GHG fluxes, where we assume the contribution of gases are derived from heterotrophic respiration of older peat C/N, root exudated C/N from adjacent plants, dissolved N in groundwater and belowground autotrophic respiration (CO_2) from roots inhabiting the peat below the collars. We are aware that omitting plants prohibit a full evaluation of the net ecosystem exchange of GHG and hence its net climate impact, as the aboveground plants represent a net sink of atmospheric CO_2 and can increase the emission of CH_4 and N_2O (Jørgensen et al., 2012; Vroom et al., 2022). However, by removing plants we isolate the soil processes leading to net soil emission/uptake of the GHG. Collectively, this can provide a mechanistic insight into the regulation of fluxes by hydrology and temperature. We acknowledge that studies of GHG fluxes in peatlands should seek to include the aboveground plant component to the net GHG flux from the ecosystem if possible.

Two months prior to collar installation in summer 2021, we cleared vegetation within and around each collar ($\sim 40 \times 40$ cm) by harvesting and applying a single recommended dose of glyphosate (~ 100 mg m^{-2}) to aboveground plants only, avoiding soil contact. Glyphosate's average half-life in mineral soils is ~ 21 d, ranging from 6–87 d and increasing with clay content (Padilla and Selim, 2020). Given the low dose and absence of clay, residual glyphosate was likely minimal during flux measurements. Although repeated applications can suppress microbial activity (Nguyen et al., 2016), the single treatment months prior suggests limited direct impact on microbial respiration. Still, transient effects cannot be ruled out, and the lack of an untreated control prevents quantification. Regrowth inside collars was manually removed at least weekly, minimizing photosynthetic CO_2 uptake. While regrowth abundance was not measured,

stable net CO_2 efflux between removals suggests minimal impact. Aboveground plant removal is standard for isolating soil GHG fluxes, though belowground autotrophic respiration from adjacent roots remained, as trenching was avoided to reduce site disturbance. Without a control plot, the direct effect of disturbance on GHG fluxes remains uncertain.

2.2 Overview of time series of GHG fluxes, soil temperature/moisture, air temperature, wind direction and groundwater level

The dataset is comprised of a 12-month time series of net soil fluxes of CO_2, CH_4 and N_2O, accompanied by a longer timeseries of soil temperature and moisture at 5 cm depth, meteorological variables (air temperature, wind speed and direction measured at 2 m height) and a shorter time series of groundwater table level, depth and temperature (Table 1). Due to equipment failure of the SkyLine2D the GHG flux measurements started on 2 February 2022 and ended 28 January 2023 in total 360 d (Table 1). Groundwater level measurements started between 9 to 31 March 2022 (Table 1). All other variables were measured continuously from 1 July 2021, until 31 January 2023 (Table 1). In the period between 7 and 19 December 2022 intermittent periods of snow cover (depth was not measured) on the ground occurred. This snow cover did not impede flux measurements.

2.3 The SkyLine2D system at Vejrumbro

The SkyLine2D system is an automated chamber based system for measuring GHG fluxes. The system is designed and built by Earthbound Scientific Ltd. (United Kingdom). We used the SkyLine2D system to measure the net soil fluxes of CO_2, CH_4 and N_2O measured with an automated GHG chamber system over 12 months resolving spatiotemporal patterns of GHG fluxes including 27 individual collars (26 on organic soil and 1 in a ditch) over a 24 m transect on a temperate drained fen peatland (Figs. 1B and 3).

The SkyLine2D system transect was oriented in a north-south direction (Fig. 1B). Two 2.5 m-tall scaffold towers marked the end of the 30 m SkyLine2D system (Figs. 1B and S2D). The towers were fixed by ropes attached to 1000 L pallet tanks filled with water (Fig. S2D) that maintained a stable position of the towers and ropes and hence placement of the chamber over the collars. The GHG analyser (model G2508, Picarro Inc., USA) was installed in a waterproof and temperature-controlled shelter at the south end of the transect (Figs. 1B and S2C). The transect was situated on the edge of the riparian fen near the mineral upland soils, where active agriculture was practiced (Fig. 1B). Along the transect volumetric soil water content (SWC) and soil temperature (ST) as well as water table depth (WTD) were measured at seven locations (Fig. 2). The agricultural field north of the SkyLine2D was sown with annual crops in rotation according to common practice.
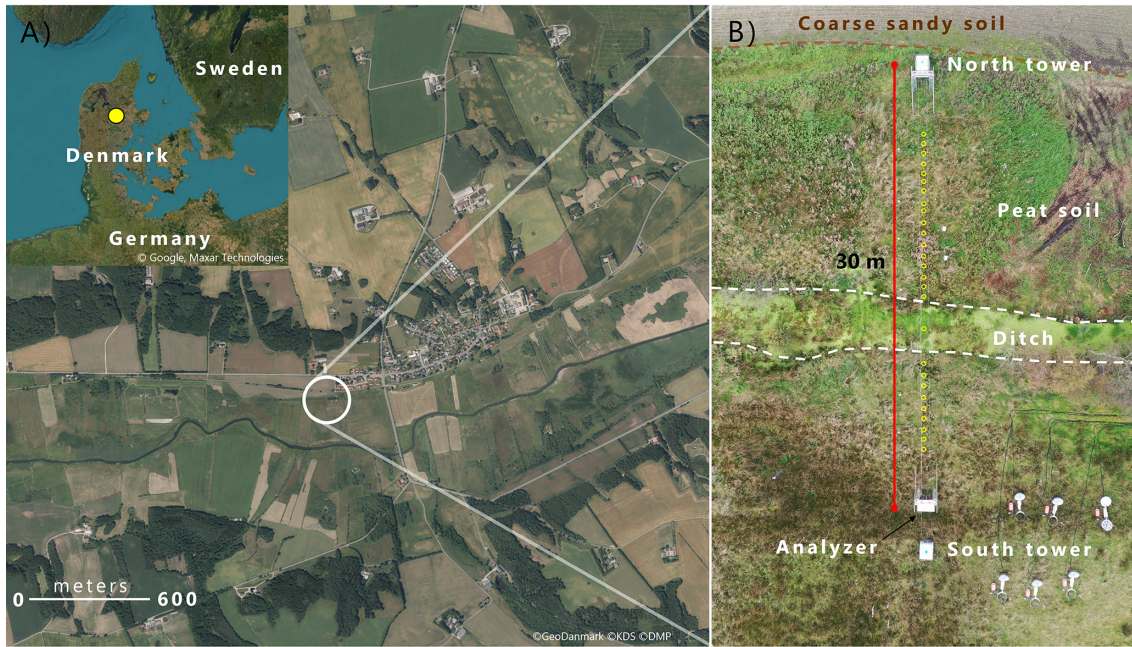
Figure 1. (A) The Vejrumbro location in Jutland (N 56.43819 E 9.54527 (WGS 84)) in the Nørre Å valley near the village of Vejrumbro. The grey circle marks the placement of the SkyLine2D system. Satellite images: © Google Earth. **(B)** Drone image of the measurement transect (27 September 2023) after flux measurements had stopped. Dashed brown line marks the approximate boundary between the agricultural field, coarse sandy soil (north) and the peat/organic soil (south). The red line marks the end points of the SkyLine2D system (30 m). The open yellow circles ($n = 27$) mark the approximate position of individual collars across the transect of the field (24 m in length) where greenhouse gas fluxes were measured. The ditch is located between the dashed white lines. The analyser was placed at the south tower. Elevation above sea level along the 24 m collar transect varied from 3.77 m in the south to 4.06 m in the north.

Greenhouse gas flux measurements with the SkyLine2D system

Along the SkyLine2D transect the 26 individual collars (Ø19 cm) along the 24 m transect on organic soil (Fig. 2) were inserted 5 cm into the peat leaving 5 cm above the surface. The collars were distanced app. 70 cm apart. One collar was installed in the ditch by inserting a tube (Ø19 cm, length 100 cm) to the bottom of the ditch with holes deeper than the minimum water level in the ditch to allow water flow. Thus, it was avoided that air entered in the collar in the ditch due to low water levels in the ditch. On top of this longer tube a collar (Ø19 cm, length 10 cm) was glued allowing for flux measurements. The chamber was programmed to stop when the bottom of the chamber reached the water surface if the water level in the ditch extended above the top of the collar. For most of the time the collar was not submerged, and the chamber therefore hit the collar.

There was one round transparent chamber (height: 39.5 cm and inner Ø: 19 cm, volume: 11.2 L) on the SkyLine2D, hanging below a moving trolley, which was suspended on two ropes stretched between the north and south towers (Fig. S2A and B). At defined positions along the rope, neodymium magnets had been inserted, and a magnet sensor (Fig. S2B) on the trolley informed the internal computer

to stop and lower the chamber over positions with a collar on the surface. The chamber was lowered and guided down to the collar by supporting rods shaping a funnel (Fig. S2A). The chamber stopped when it hit the collar, achieved through a pressure sensor on top of the chamber connected to a hollow rubber gasket (Ø 3 cm) at the bottom, which also sealed the chamber with the collar. There was no fan installed in the chamber as the mixing was ensured by the main pump (Fig. S2C). A vent was installed in the top of the chamber to allow for pressure equilibration under windy conditions and chamber deployment.

One entire flux + flushing sequence lasted 10 min (Table 1). The chamber closure period was set to 5 min with a purging time of 5 min in between measurements when chamber was open and hanging underneath the trolley at approximately 1 m above the ground (Fig. S2D). This provided on average 10 min between flux measurements on consecutive collars (Table 1). Due to small variations in mechanical operations, flux measurements were occasionally farther apart than 10 min, but overall, the timing of the SkyLine2D system was consistent. After each cycle of 27 flux measurements there was a 30 min delay until the start of the next cycle. On average this resulted in 4–5 flux measurements per collar per day throughout the period.
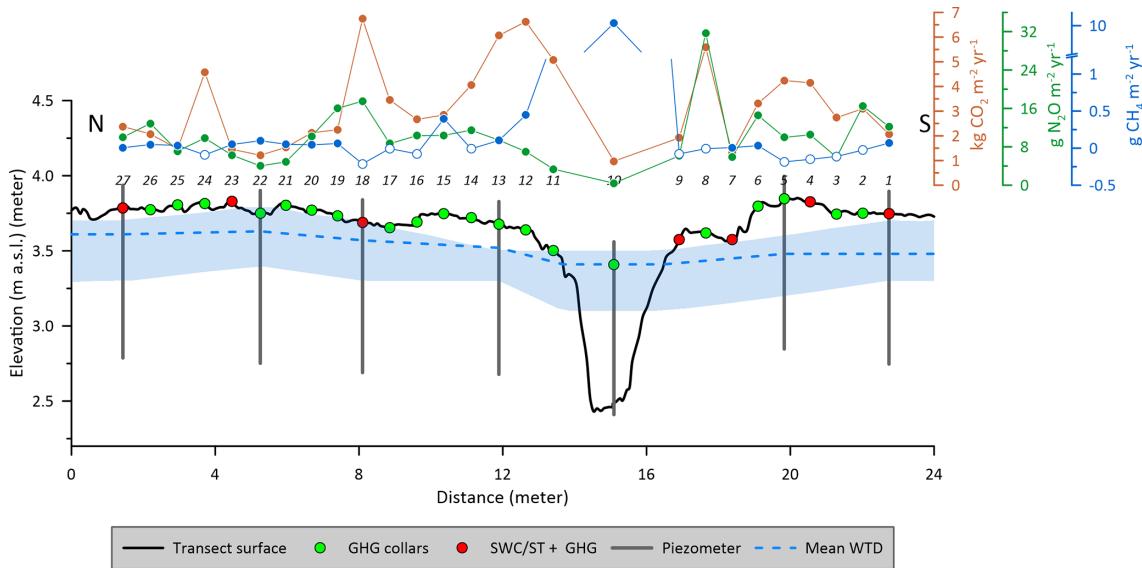
Figure 2. Schematic representation of the measurement transect at Vejrumbro and associated measurement variables. The annual cumulative fluxes of CO_2 (red) (kg CO_2 m^{-2} yr^{-1}), N_2O (green) (g N_2O m^{-2} yr^{-1}) and CH_4 (blue) (g CH_4 m^{-2} yr^{-1}) are shown for each collar across the measurement transect at Vejrumbro. Closed and open symbols for CH_4 represent net cumulative emission and uptake, respectively. Mean groundwater level is the mean water table elevation measured in piezometers (blue dashed line) with shaded blue area represent maximum and minimum observed groundwater elevation. GHG collars (green symbols) mark the positions of greenhouse gas flux measurements of CO_2, CH_4 and N_2O. SWC/ST + GHG mark the positions where volumetric soil water content (SWC) and soil temperature (ST) at 5 cm depth were measured alongside greenhouse gas fluxes. Numbers on top of plot show the collar numbers (from 1–27). N and S mark the north and south ends of the transect (see Fig. 1B). The peat depth was at least one meter in all points. Elevation is given meters above sea level (m a.s.l.).

To determine the concentrations of CO_2, CH_4 and N_2O in the chamber air, a laser spectroscopy GHG analyser (model G2508, Picarro Inc., USA) was used. The sample output frequency was set to 1 Hz with a manufactured specified raw precision on 1 Hz data for CO_2: 240 ppb, CH_4: 0.3 ppb and N_2O: 5 ppb at ambient conditions (Picarro Inc., USA). A main pump (model: N86 KN.18, KNF, Germany) circulated the air to and from the chamber at 6 L min^{-1}. The GHG analyser was installed in parallel to the inflow from the chamber due to the much lower flow of 250 mL min^{-1} of the vacuum pump. There was a 30 m tube between the chamber and main pump to allow for the GHG analyser to remain stationary in the hut while the trolley moved.

2.4 Peat sampling and analysis

In November 2023 the peat across the SkyLine2D transect was sampled to 1 meter depth using a Russian auger and cores split into five layers of 20 cm thickness. Collars 1, 2, 5, 6, 8, 13–27 were sampled (Fig. 2). For the remaining collars it was not possible to retrieve a sample due to excessive wetness of the peat. The decomposition of the peat samples were assessed by a 10-point Von Post scale of humification (1 = completely undecomposed and 10 = completely decomposed) together with pH$_{H_2O}$ determined by suspending peat in demineralized water (1 : 5 peat : watermix), dry

bulk density (g cm^{-3}) and total C and N by dry combustion (g C/N 100 g peat^{-1} or %).

2.5 Groundwater table level, depth and sampling

To measure the groundwater level piezometers (inner diameter 5 cm) were installed at collars 1, 5, 10 (ditch), 13, 18, 22, 27 (Fig. 2) to 1 m depth below the surface, which is deeper than the lowest groundwater level in summer ($\sim$ 60 cm below the surface) with openings from 0.1–1.2 m below terrain. In the ditch the piezometer bottom was deeper than one meter to secure anchoring in the peat. The piezometers were installed approximately 50–60 cm beside the collars to avoid interference with the SkyLine2D system. After installation, piezometers were cleaned and sealed at the surface with bentonite pellets to avoid surface infiltration along the piezometers which can distort water level measurements.

Pressure transducers (Table 1) connected to Arduino-loggers were installed in each piezometer (at collars 1, 5, 10, 13, 18, 22 and 27 – Fig. 2) approximately 1 m below terrain measuring water levels every 15 min. The pressure transducers were vented and thus do not need correction for atmospheric pressure.

The groundwater levels were described using two metrics: hydraulic head and groundwater table depth (WTD). Hydraulic head represents the water level relative to mean

Table 1. Available time series data from the Vejrumbro SkyLine2D system. Coloured Data availability for each variable in 2021 to 2023 is indicated with horizontal bars.

Variable	Unit	Model/sensor type	Frequency (minutes)	2021	2022	2023
CO_2 flux[a]	$\mu mol\ CO_2\ m^{-2}\ s^{-1}$	G2508 (Picarro Inc., USA)	$\sim 10^b$			
CH_4 flux[a]	$nmol\ CH_4\ m^{-2}\ s^{-1}$	G2508 (Picarro Inc., USA)	$\sim 10^b$			
N_2O flux[a]	$nmol\ N_2O\ m^{-2}\ s^{-1}$	G2508 (Picarro Inc., USA)	$\sim 10^b$			
Soil temperature at 5 cm depth[c]	°C	RXW-TMB-868 (Onset, USA)	5			
Soil water content at 5 cm depth[c]	$(cm^3\ cm^{-3})$	RXW-SMD-868 (5HS) (Onset, USA)	5			
Air temperature at 2 m height	°C	S-THC-M002 (Onset, USA)	5			
Wind speed	$m\ s^{-1}$	S-WSB-M003 (Onset, USA)	5			
Wind direction	°	S-WDA-M003 (Onset, USA)	5			
Groundwater level[d]	m a.s.l.	DCL532 (BD sensors, Germany)	15			
Groundwater table depth[d]	cm	DCL532 (BD sensors, Germany)	15			
Groundwater temperature[d]	°C	Dallas DS 18B20	15			

(Months indicated across columns: 2021 – Aug, Sep, Oct, Nov, Dec; 2022 – Jan, Feb, Mar, Apr, May, Jun, Jul, Aug, Sep, Oct, Nov, Dec; 2023 – Jan)

[a] Net soil/ditch fluxes for all collars 1–27. [b] Time in between two consecutive flux measurements. The 10 min comprise actual flux measurement of 5 and 5 min headspace flushing between flux measurements.
[c] Measured for a subset of collars: 4, 7, 9, 23, 27. [d] Measured for a subset of collars: 1, 5, 10 (ditch), 13, 18, 22, 27.

sea level, based on the Danish Vertical Reference (DVR90), while WTD indicates the depth of the groundwater below the surface terrain and represented in positive values, where WTD of zero is equivalent to groundwater level at the terrain surface. The elevation of top of the piezometers were measured using a GPS (model GS07 High Precision GNSS Antenna with a CS20 Controller, Leica, Germany) and used as a local reference for hydraulic head. Manual measurements of groundwater levels were conducted every 2 months and used to calibrate the logger water levels to hydraulic head and WTD.

Groundwater water sampling and chemical analysis

Groundwater was sampled monthly in the piezometers placed at collars 1, 5, 13, 18, 22 and 27 (Fig. 2) by retrieving a 200 mL sample 20–30 cm below the groundwater level at the sampling time. The water sample was retrieved using a syringe and transferred to a plastic bottle that was capped immediately to avoid echange with the atmosphere and contamination. Water samples were frozen immediately after sampling and subsequently after thawing analyzed for pH, EC and alkalinity on an 855 Robotic Titrosampler (Metrohm, Germany). Total N and DOC were measured on a TOC-V CPH Analyzer with Total Nitrogen Unit TNM-1 & ASI-V Autosampler (Shimadzu, Japan). Ion chromatograph (IC) analyses of Cl^-, NO_3^-, and SO_4^{2-} were performed on a 930Compact IC Flex (Metrohm, Germany) and NH_4^+ concentrations were measured with continuous flow analysis using a Seal AA500 Autoanalyzer (SEAL Analytic, USA). Total dissolved Fe and P were analyzed with coupled plasma–mass spectrometry (ICP-MS) on an iCAP-Q ICP-MS (Thermo Fisher Scientific, USA) in KED mode using He as the collision gas. Prior to analysis the 10 mL subsamples were acidified with 200 μL concentrated nitric acid. Elemental ICP-MS analyses also included dissolved base cations of Ca^{2+}, Mg^{2+}, K^+, Na^+ as well as total dissolved Al and Mn cations (not shown but included in the data set).

2.6 Soil moisture and temperature measurements

Soil moisture and temperature probes were initially inserted for collars 1, 4, 7, 9, 18, 23, 27 (Fig. 2) in order to obtain a representation of the entire transect. Soil moisture probes (6 cm length) were inserted at an approximate 30° angle 5 cm outside the collar, while the soil temperature probes were inserted vertically adjacent to the soil moisture probe. Due to sensor failures soil moisture was measured for collars 1, 7, 9, 18, 23 and 27 and soil temperature at 4, 7, 9, 23 and 27.

2.7 Wireless data transfer

Wireless sensors for air temperature, wind speed, wind direction, soil temperature and volumetric soil water content were set up with Wi-Fi data transfer to HOBO RX3000 Weather

Station (Onset, USA) equipped with HOBOnet Manager (RXMOD-RXW-868) module for wireless communication with sensors and logged data every 5 min. Data access was through the HOBOlink cloud software.

Groundwater loggers were interfaced with the I^2C (Inter-integrated Circuit) protocol and data was collected on Arduino custom-built logger (https://vandstande.dk/logger.php, last access: 24 November 2025) with wireless connection via LoRaWANor SigFox.

2.8 Calculation of diffusive fluxes

Fluxes were calculated and quality checked using the goFlux R package (Rheault et al., 2024) and presented as $\mu mol\, CO_2\, m^{-2}\, s^{-1}$, $nmol\, N_2O\, m^{-2}\, s^{-1}$ and $nmol\, CH_4\, m^{-2}\, s^{-1}$. Prior to flux calculations, the gas concentration data from the G2508 analyzer was matched to the chamber closure time and chamber id to determine the start time of the chamber measurement, so it was possible to separate individual flux measurements from each collar over the measurement time (see examples of flux detection and calculation in Fig. S3A–D). An automatic deadband detection method was applied based on maximal R^2 of a linear regression over the first 180 s (in 10 s steps) after chamber closure. The deadband was allowed to attain values between 0 to 150 s thereby also allowing for compensation for the ~ 60 s delay between chamber headspace gas concentration change and GHG analyser detection due to transport time through the 30 m tube connecting the chamber and GHG analyser.

Flux calculations were done with both linear (LM) and non-linear (Hutchinson-Mosier – HM) regression models (Pihlatie et al., 2013) to determine the slope at time zero. The best flux estimates with either the LM or HM regression model was determined using the *best.flux* function in the goFlux package (Rheault et al., 2024). Shortly, if the RMSE of the HM model was lower than minimum detectable flux (MDF), HM was chosen. However, if the ratio (called g-factor) between HM and LM was larger than 2, LM was chosen, as this indicates over-fitting of the HM, which may result in unrealistic large HM flux estimates. If the relative SE of the slope (SE/slope) at time zero for the HM model was larger than 100 % it indicated overfitting of the HM model and the LM was chosen. This approach is conservative as it will discard non-linear flux behaviour and instead provide a conservative linear flux estimate. Out of 47.438 detected flux measurements for CO_2, CH_4 and N_2O, respectively, a total of 2807 CO_2 fluxes (5.9 %), 3339 N_2O fluxes (7 %) and 4923 CH_4 fluxes (10.3 %) were discarded due to the following two situations: (1) chamber mechanical malfunction either resulting in imperfect sealing on collar due to erroneous lowering of chamber on collar indicated by background atmospheric or fluctuating gas concentrations in the headspace and (2) at *in situ* flux levels close to the minimum detectable flux of the Picarro G2508 analyser (Christiansen et al., 2015)

non-significant regression (between concentration and time and GHG concentration) ($p > 0.05$) were also discarded as it was not possible to statistically distinguish whether there was a real flux or the lack of significant regression was because of chamber malfunction. It is acknowledged that discarding low fluxes can bias annual means and cumulative values, but the data quality did not allow us to determine whether the flux measurement was performed correctly and hence a conservative approach was chosen as including false low fluxes would also bias the data set.

For flux measurements the air temperature in 2 m was used as an estimate of the chamber headspace temperature along with a 1 atm air pressure.

The annual cumulated fluxes from the soil or the ditch (diffusive only) were estimated simply by multiplying the daily average CO_2, CH_4 or N_2O flux for the measurement period with 365 d. We believe for the purpose of data presentation that this simplistic methodology is adequate here, also given the very few data gaps in the timeseries. However, there are other more sophisticated methods using interpolation and response variable functions that may refine the annual budget. However, it is not the goal of this manuscript to present these methodologies but to provide the data so other users can test different temporal upscaling methodologies.

2.9 Calculation of ebullition fluxes in the ditch

Methane ebullition fluxes were occasionally observed only in the ditch. The resultant CH_4 time series for the chamber would have a characteristic appearance (Fig. S4) where the measurement would essentially start out as diffusive flux measurement, then CH_4 bubbles entered the chamber headspace, and the concentration would quickly increase to a maximum value and reach a threshold concentration corresponding to the mixed headspace concentration. In these cases, the LM/HM flux calculation assumptions are violated and instead the ebullition flux would be calculated as the total increase in CH_4 mass m^{-2} per 5 min enclosure. The mass flux of CH_4 per enclosure ($nmol\, m^{-2}$ per 5 min enclosure) was calculated according to Eq. (1):

$$F_{CH_4-ebu} = dCH_4 \cdot \frac{V_{system} \cdot P}{A \cdot R \cdot T} \tag{1}$$

Where dCH_4 is the concentration difference in nmol between start of chamber enclosure ($CH_{4,start}$) and end CH_4 concentration ($CH_{4,end}$) after it reached a plateau (Fig. S4), V_{system} is the total volume (11.7 L) of the system (collar, chamber, tubes and GHG analyser) in L, P is the pressure (1 atm), A is the area of the collar (0.028 m^2), R is the gas constant (0.082057 $L\, atm\, K^{-1}\, mol^{-1}$) and T is the chamber headspace temperature (K). To calculate the ebullition flux per second the ebullition flux estimate was divided by $12 \cdot 60$ s (300), equivalent to the number of seconds over the 5 min measurement period.

Out of a total of 1728 flux measurements from the ditch (collar 10), 334 were classified as ebullitions according to our definition above. indicating that ebullition was erratic which is in line with studies of ebullition of fluxes from ponds (Sø et al., 2023; Wik et al., 2016). Hence, it can be assumed that ebullition occurred around 19.3 % of the time during the measurement period (360 d). An annual estimate of the ebullition flux was calculated as the average ebullition flux in $\mathrm{nmol\,CH_4\,m^{-2}\,s^{-1}}$ by multiplying with number of seconds over 365 d and the 19.3 % during period where ebulittion occurred.

Ebullitions could also be caused by mechanical disturbance of the chamber landing on the collar. Ebullition fluxes were discarded if the sudden increase in CH_4 headspace concentration (Fig. S4) occurred 60 s after recorded chamber closure as this indicated bubbles released by chamber deployment on top of the collar.

3 Data presentation

3.1 Wind speed and direction

Generally, the wind regime during the measurement period (2 February 2022 to 28 January 2023) was rather mild with monthly average wind speeds ranging between 1.2 to 2.9 m s^{-1} and maximum gust up to 20 m s^{-1}. The wind direction was uniformly from the west for 52 % of the time, with easterly winds constituting 27 % and northern and southern winds 8 % and 13 % of the time (Fig. 3). Winds from western directions were highest for the longest period, while easterly winds were of similar magnitude, but less frequent (Fig. 3). Northern and southerly winds were generally below 3 m s^{-1} and represented periods with still conditions. The very uniform western-eastern wind field at Vejrumbro may also partly be explained by the W-E direction of the valley in which the site is situated, that effectively blocks or dampens winds from S and N.

3.2 Air and soil temperature

Over the study period the average air temperature was 9.6 °C ranging between maximum 37.9 °C and minimum of −18.6 °C (Fig. 4A). Monthly ranges of air temperatures (Table 2) show >20 °C variation between minimum and maximum, except for February, pointing towards large diurnal variations. Soil temperature magnitude and temporal variation were similar across the transect, varying between 0 to 28 °C (Fig. 4B) and followed that of air temperature (Fig. 4A) with less variability (Fig. 4B and Table 2). The annual site average soil temperature was similar to the air temperature (Table 2).

3.3 Groundwater table depth

Average groundwater table depth (WTD) below terrain during the period was between 47 to 21 cm across the transect (Fig. 2, Table 2). During summer, the peat drained between 18–31 cm below the annual average and in winter the WTD increased to 0–22 cm above the annual average across the transect (Fig. 2, Table 2). Generally, the WTD elevation was lower in the ditch across the entire study period (Fig. 2). It was only on the northern end of the transect that the surface occasionally was flooded during winter periods (Fig. 2).

The temporal variability of WTD was similar across the transect despite different absolute water table depths (Fig. 5A–F). In the summer periods, the WTD was most variable decreasing to below 40 cm for collars 1, 13, 18, 22 and 27, whereas the WTD for collar 5 showed the deepest WTD measured over the transect. WTD responded quickly (within hours) to precipitation events that could increase the WTD by almost 40 cm at some plots, indicating that the entire aerated soil volume above the groundwater table was flooded. There was a slight tendency to lower response to precipitation events for piezometers at collar 5 and collar 13 that were placed closer to the ditch (Figs. 2 and 5B and C). As the ditch water level was lower than in the peat this could be explained by more efficient lateral drainage into the ditch from the areas closer to the ditch. In the winter periods, the WTD was less responsive to precipitation and was closer to the surface (Fig. 5A–F) across the transect.

3.4 Soil water content

Due to instrument failure the temporal coverage of soil moisture in the topsoil (5 cm) was not similar across the transect (Fig. 6A–F). For collars 18, 23 and 27 the entire period of greenhouse gas measurements was covered by soil moisture measurements (Fig. 6D–F). While SWC for collars 1, 9, 18, 23 and 27 was similar in the winter periods (around 0.55 cm^3 cm^{-3}) the SWC for collar 18 decreased to lower minima between 0.1–0.2 cm^3 cm^{-3}, than the minima observed between 0.3–0.4 cm^3 cm^{-3} for collars 23 and 27 in the summer periods (Fig. 6, Table 2). Similar for all collars it was observed that SWC was more variable in summer, responding similarly as WTD to precipitation events (Fig. 6, Table 2). Since plants were removed regularly from the collars the decrease of SWC for collar 18 cannot be explained by plant transpiration, and the dynamic behaviour could indicate the impact of soil evaporation, but the different levels of SWC also show that there is spatial variation across the transect in the water retention properties of the peat soil that will impact the rate of drying. However, it cannot be ruled out that the SWC sensor at collar 18 experienced malfunction or that soil contact was lost in the dry periods of 2022 (Fig. 6D) which could lead to erroneous and too low SWC. Therefore, these data should be considered with care.
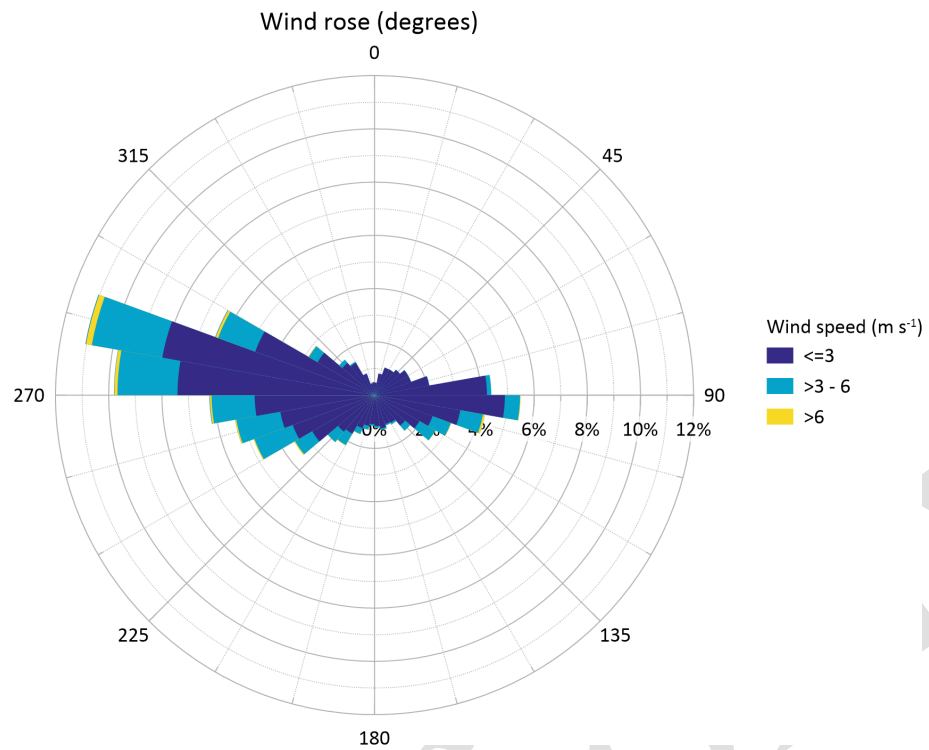
Figure 3. Wind regime at Vejrumbro for the period 1 July 2021 to 31 January 2023 presented as a wind rose diagram with wind speed and direction for the period.
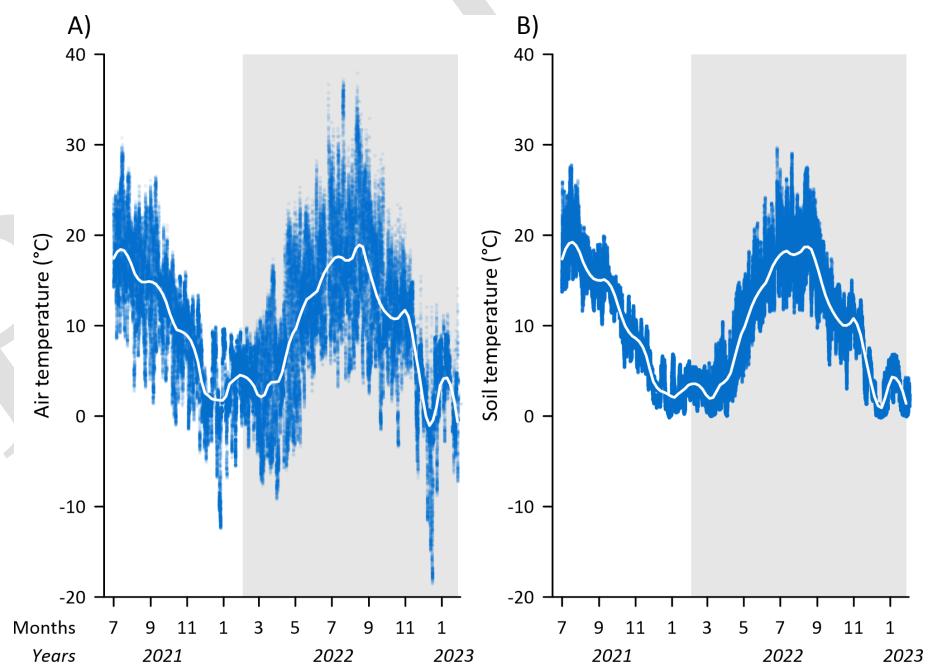
Figure 4. Time series of **(A)** air temperature in °C measured at 2 m height above the surface and **(B)** soil temperature (°C) at 5 cm depth for collars 4, 7, 9, 23 and 27 along the measurement transect. The blue dots are the raw 5 min measurements of air temperature and the white lines represent LOESS fit to show overall seasonal trend. The periods of GHG measurements with the SkyLine2D system are shown with the shaded area.

Table 2. Monthly mean, maximum and minimum air temperature and soil temperature (°C), groundwater table depth (cm) and volumetric soil water content ($cm^3\,cm^{-3}$) at Vejrumbro in the measurement period from 1 February 2022 to 31 January 2023.

Variable	Year Month	Feb	Mar	Apr	May	Jun	Jul	Aug	Sep	Oct	Nov	Dec	Jan	Avg
							2022						2023	
Air temperature (°C)	Mean	3.8	3.0	6.6	12.0	15.4	17.7	16.6	13.4	10.7	6.9	1.2	3.7	9.6
	Max	10.6	17.4	23.7	25.3	36.7	37.2	37.9	32.9	23.3	18.4	12.4	14.1	–
	Min	−4.3	−9.3	−8.3	−3.4	4.3	3.2	2.7	−1.5	−3.5	−6.9	−18.6	−7.3	–
Soil temperature (°C)	Mean	3.0	3.2	2.9	6.4	12.3	16.1	18.4	17.0	13.8	10.3	7.2	2.1	9.6
	Max	6.5	5.3	9.1	12.5	18.8	25.1	27.0	24.7	19.3	14.3	12.6	6.3	–
	Min	0.3	1.1	0.4	0.8	6.6	10.7	12.4	11.8	7.0	4.0	2.1	0.0	–
Groundwater table depth (WTD) (cm)	Mean	–	39	35	41	36	41	35	31	20	18	17	13	29
	Max	–	58	39	58	43	52	46	36	30	31	28	28	–
	Min	–	23	5	24	9	28	22	9	5	6	3	2	–
Volumetric soil water content ($cm^3\,cm^{-3}$)	Mean	0.53	0.45	0.40	0.37	0.38	0.43	0.43	0.45	0.50	0.53	0.52	0.51	0.46
	Max	0.56	0.51	0.50	0.41	0.47	0.55	0.56	0.56	0.57	0.58	0.56	0.57	–
	Min	0.43	0.39	0.37	0.33	0.32	0.26	0.32	0.35	0.40	0.47	0.42	0.34	–

3.5 Peat soil characteristics

Generally, there was peat/organic soil to one meter depth except for one collar (25) where gyttja was found in a depth of 80 cm (Table 3). The organic soil was more decomposed in the top 40 cm indicated by higher Von Post values between 5 and 10. Below 40 cm peat still displayed high levels of decomposition along the transect, but was more often found to be less decomposed, values ranging from 1–8 (Table 3). This corresponds well to the previous land use with drainage of the topsoil leading to higher degree of humification. Also, the organic soil was most dense in the top 20 cm (on average $0.31 \pm 0.02\,g\,cm^{-3}$) and bulk density decreased to 0.10–$0.12\,g\,cm^{-3}$ from 40–100 cm depth. Total C and N was lowest in the 0–20 cm layer, but still classified as organic soil. Below 20 cm total C and N concentrations, respectively were similar. C/N ratio was lowest in the top 20 cm (16 ± 0.4) and increased to 22–25 in 20–100 cm depth (Table 3).

3.6 Groundwater and ditch water chemical composition

Site mean pH of the groundwater in the organic soil was 5.8 ± 0.1 and was lower than the pH of the ditch (7.3 ± 0.6). There was a tendency towards lower pH in groundwater and ditch towards the end of the measurement period (Fig. 7A). Electric conductivity was generally higher in the ditch water ($359 \pm 36\,\mu S\,cm^{-1}$) compared to the groundwater in the organic soil ($276 \pm 18\,\mu S\,cm^{-1}$) but varied less over the season. The groundwater shows a clear peak in EC around September 2022 (Fig. 7B). Total dissolved P was markedly higher in the groundwater ($687 \pm 45\,\mu g\,P\,L^{-1}$) compared to the ditch water ($76 \pm 10\,\mu g\,P\,L^{-1}$). Whereas there was little seasonal trend in ditch P concentrations, dissolved P in groundwater dipped to below average concentrations between August to October, likely indicating plant uptake

during the growing season (Fig. 7C). Similarly, total dissolved N was higher in groundwater ($6.7 \pm 0.5\,mg\,N\,L^{-1}$) than in ditch ($2.6 \pm 1.6\,mg\,N\,L^{-1}$) with increasing concentrations during the growing season (Fig. 7D). This temporal trend was also observed for NO_3^- (Fig. 7E), but average groundwater ($2 \pm 0.5\,mg\,NO_3\text{-}N\,L^{-1}$) and ditch ($2.2 \pm 1.5\,mg\,NO_3\text{-}N\,L^{-1}$) concentrations were similar. As expected, dissolved NH_4-N was lowest among investigated N-species and there was more dissolved NH_4-N present in groundwater ($0.8 \pm 0.1\,mg\,NH_4\text{-}N\,L^{-1}$) than in the ditch ($0.14 \pm 0.25\,mg\,NH_4\text{-}N\,L^{-1}$). However, there was no discernable temporal trend for NH_4^+ (Fig. 7F). Collectively, the temporal trend of TN and NO_3^- could point to temperature driven mineralization of the peat. Also, the organic N (TN – inorganic N-species) was on average 10 times higher in the groundwater than in the ditch. Average SO_4^{2-} concentrations were similar between the groundwater ($17.5 \pm 2.4\,mg,SO_4\text{-}S\,L^{-1}$) and ditch ($17 \pm 1.5\,mg\,SO_4\text{-}S\,L^{-1}$), but SO_4^{2-} concentration peaked during September and October in the groundwater whereas it remained more constant in the ditch over the season (Fig. 7G). Like the dissolved organic N, DOC concentrations were consistently higher in the groundwater ($73 \pm 3.1\,mg\,DOC\,L^{-1}$) than in the ditch ($9.4 \pm 3.5\,mg\,DOC\,L^{-1}$), but peaked later in the season, around December 2022, whereas there was little temporal variability of DOC in the ditch (Fig. 7H). Dissolved total Fe displayed the same temporal trend as DOC (Fig. 7I) but was higher groundwater ($1916 \pm 163\,\mu g\,Fe\,L^{-1}$) compared to the ditch ($98 \pm 95\,\mu g\,Fe\,L^{-1}$). The geochemical parameters of groundwater and ditch water point to different mechanisms regulating peat decomposition and possibly plant uptake, where the chemical composition of groundwater varied more over time than ditch water. Generally, there were no
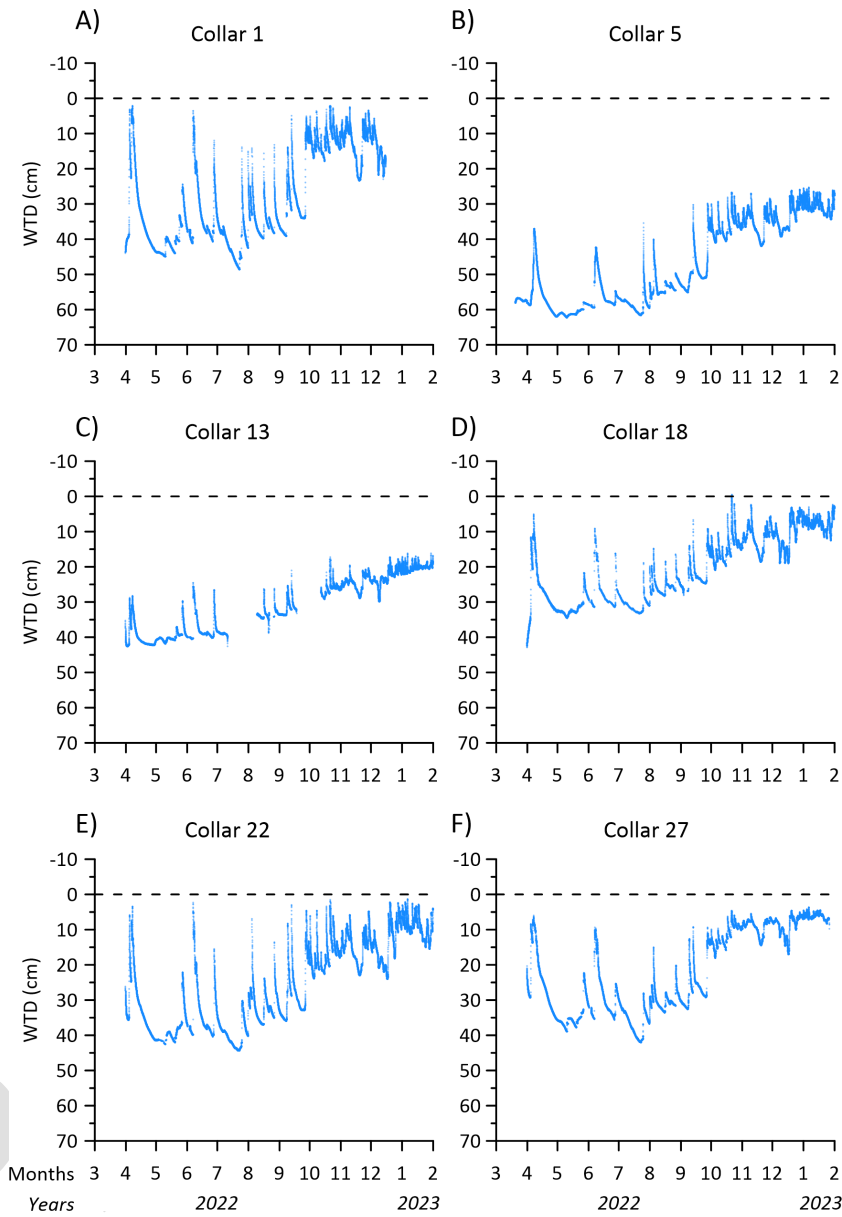
Figure 5. Time series of groundwater table depth (WTD) below terrain for the six piezometer locations along the SkyLine2D transect in the period 31 March 2022 and 31 January 2023 when the flux measurements stopped. Dashed line show surface.

Table 3. Mean (± standard error of the mean (SE)) peat/organic soil characteristics of humification degree (Von Post), pH (H_2O), dry bulk density (ρ_{dry}), total C (TC) concentration, total N concentration (TN) and the C/N ratio for collars 1, 2, 5, 6, 8 and 13–27 at the Vejrumbro transect.

		Von post		pH (H_2O)		ρ_{dry} (g cm^{-3})		TC (%)		TN (%)		C/N	
Depth (cm)	N	Min	Max	Mean	±SE	Mean	±SE	Mean	±SE	Mean	±SE	Mean	±SE
0–20	20	7	10	4.2	0.08	0.31	0.02	26	1.1	1.6	0.06	16	0.4
20–40	20	5	10	4.6	0.06	0.20	0.01	43	1.3	1.8	0.04	24	0.7
40–60	11	3	8	4.9	0.10	0.15	0.01	48	1.8	1.9	0.05	25	1.1
60–80	11	3	6	5.3	0.09	0.11	0.01	47	1.8	1.9	0.05	24	0.6
80–100	10	1	8	5.4	0.09	0.10	0.02	44	2.1	1.9	0.05	24	0.6
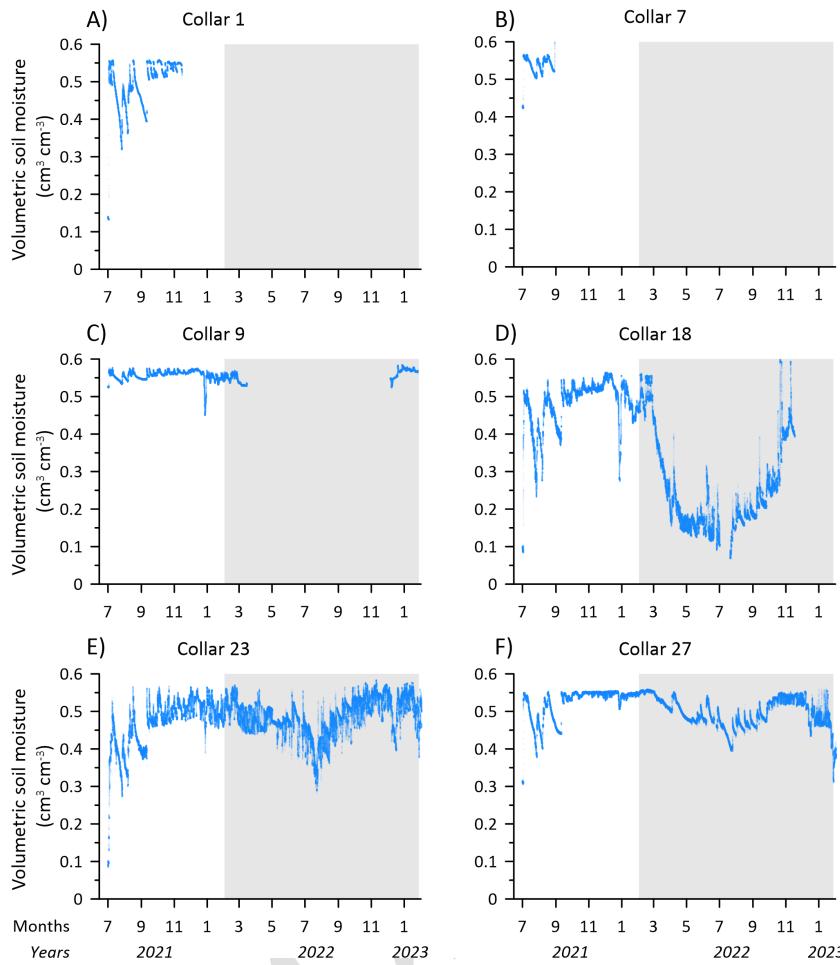
Figure 6. Time series of volumetric soil water content ($cm^3 cm^{-3}$) in 0–5 cm for the six collars 1, 7, 9, 18, 23 and 27 along the Sky-Line2D transect in the period 1 July 2021–31 January 2023 when the measurements terminated. The periods of GHG measurements with the SkyLine2D system are shown with the shaded area.

systematic spatial pattern of groundwater chemistry across the transect.

3.7   Net soil and ditch CO_2, CH_4 and N_2O fluxes

3.7.1   Spatial variation of net soil CO_2, CH_4 and N_2O fluxes

Within the transect, cumulative CH_4 fluxes over the study period (360 d) varied between -0.21 to 1.48 g CH_4 m^{-2} over the study period, with a transect average ($\pm$SE) cumulative flux of 0.07 ± 0.06 g CH_4 m^{-2} (Figs. 2 and 8A). Out of the 26 collars, excluding the ditch collar, 11 displayed a net uptake over the measurement period and the remaining were small net emitters (Figs. 2 and 8A). There was generally little spatial variation in the absolute CH_4 fluxes among the soil collars, but three collars (11, 12 and 15) showed increasing net positive cumulative fluxes towards the ditch (Fig. 2). The low spatial and similar temporal variation between collars indicate both hydrological indicators of SWC and WTD are poor

predictors of CH_4 fluxes across the transect. However, as we excluded plants from the collars we might have decreased the net emission of CH_4 directly by restricting gas transport in aerenchyma from deep peat layers potentially sustaining net CH_4 emission even though the observed growing season WTD was 20–40 cm (Askaer et al., 2011; Vroom et al., 2022) and indirectly by potentially reducing plant carbon supply to methanogens. The lack of consistent hot moments of CH_4 emissions, low cumulative emissions during periods of shallow WTD in the growing season (Fig. 5A–F) is in line with the measured free NO_3^-, SO_4^-, and Fe ions (Fig. 7E, G, I) in the groundwater. It is well known that the presence of other electron acceptors, such as sulphur, iron and nitrate, inhibit CH_4 production (Bridgham et al., 2013), in turn limiting net CH_4 emission. Also, the often deeper WTD in the summer between ~~TSI~~ to 40 cm below terrain also suggest that CH_4 oxidation could aid to reduce net CH_4 emission from the peat (Christiansen et al., 2016).
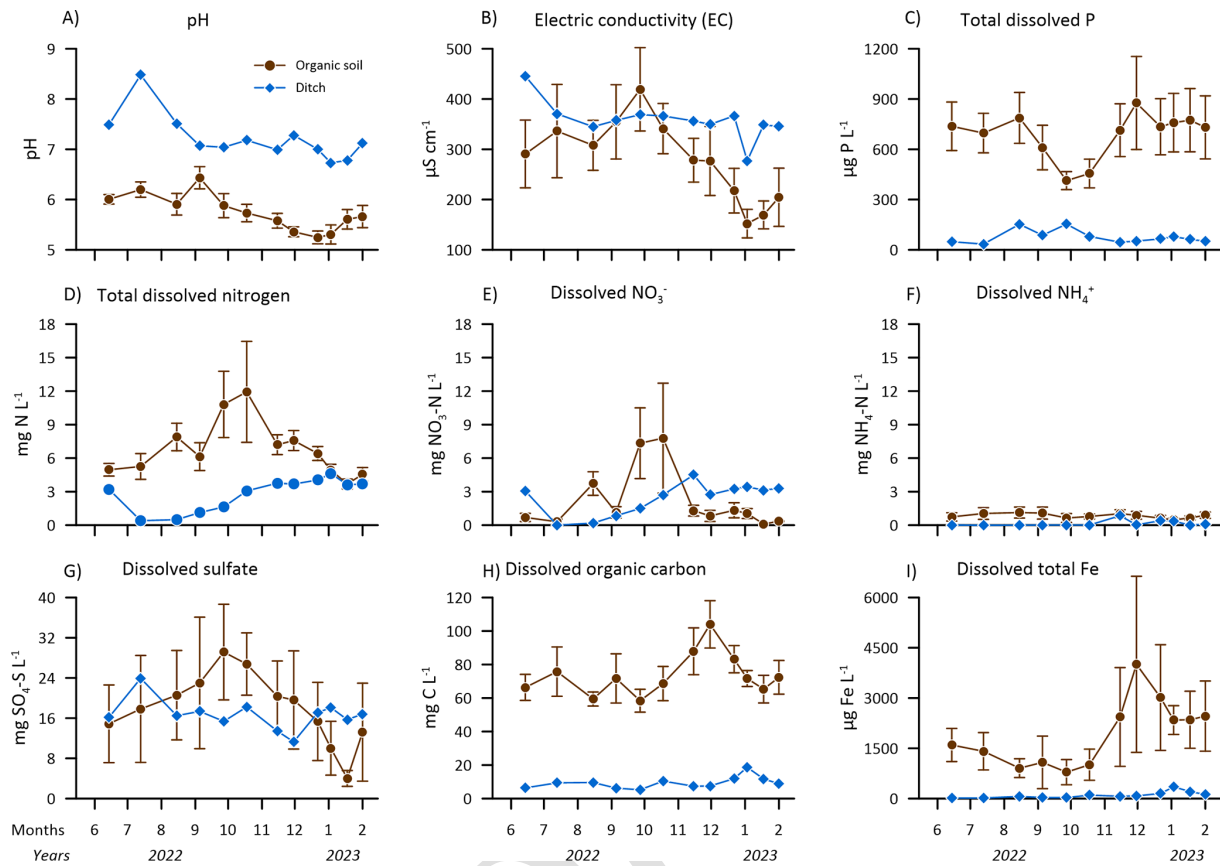
Figure 7. Groundwater (brown closed circles) and ditch water (closed blue diamonds) chemistry at Vejrumbro for the period June 2022 to February 2023 for **(A)** pH, **(B)** Electric conductivity and dissolved **(C)** total phosphor (P), **D)** total nitrogen (N), **(E)** nitrate (NO_3^-), **(F)** ammonium (NH_4^+), **(G)** sulfate (SO_4^{2-}), **(H)** organic carbon and **(I)** total iron (Fe). Values for organic soils are means for the transect with error bars showing the standard error of the mean ($N = 6$ per sampling date).
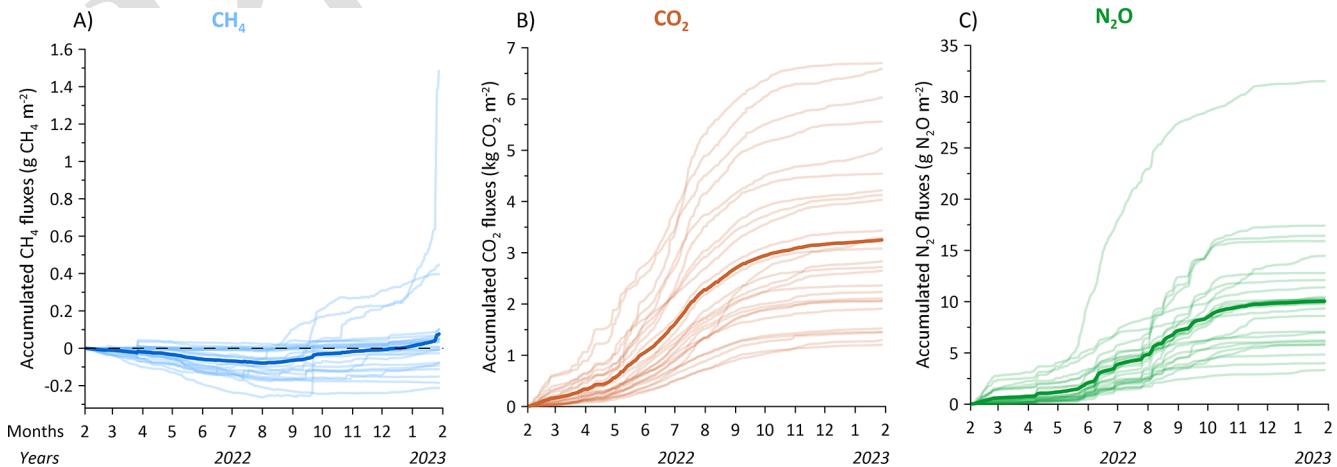
Figure 8. Cumulative fluxes of **(A)** CH_4, **(B)** CO_2, and **(C)** N_2O for 26 individual collars along the SkyLine2D transect in the measurement period February 2022 to January 2023. Units for CH_4 and N_2O are in $g\,CH_4/N_2O\,m^{-2}$ and for CO_2 in $kg\,CO_2\,m^{-2}$. The cumulative fluxes represent the raw dataset. The ditch data was excluded. Transect average is shown as thick lines.

The CO_2 effluxes displayed tremendous spatial variation across the 24 m transect (Figs. 2 and 8B) and measurements indicated that the organic soil was a net source of CO_2, with cumulative fluxes over the study period ranging between 1214–6740 $g\,CO_2\,m^{-2}$, and a transect average ($\pm$SE) of $3269 \pm 328\,g\,CO_2\,m^{-2}$, over the study period of 360 d (Figs. 2 and 8B). There was no apparent relation between the magnitude of cumulative CO_2 efflux to the position along the transect and average WTD (Fig. 2). The cumulative net soil CO_2 emission is equal to 8.9 tCO_2-$C\,ha^{-1}\,yr^{-1}$ (range of 3.3 to 18 tCO_2-$C\,ha^{-1}\,yr^{-1}$ across the transect) and compares well to estimates of annual soil C loss (8.8 tCO_2-$C\,ha^{-1}\,yr^{-1}$) from a drained unfertilized grassland on organic soil in Denmark (Kandel et al., 2018) as well as annual carbon budgets of similar Danish, British and German wetlands (Evans et al., 2021; Koch et al., 2023; Tiemeyer et al., 2020).

Similarly, the partcular site at Vejrumbro where the SkyLine2D was located was overall a net source of N_2O, with cumulative fluxes ranging between 3.3–32 $g\,N_2O\,m^{-2}$, with a transect average ($\pm$SE) of $10.1 \pm 1.1\,g\,N_2O\,m^{-2}$ (Figs. 2 and 8C) over the study period (360 d). Thus, there is a 10-fold difference between minimum and maximum cumulative N_2O fluxes within the transect, without any apparent relation to the position along the transect and WTD. The highest cumulative N_2O fluxes occurred at collar 8 situated close to the ditch (Fig. 2).The transect average cumulative N_2O emission is equivalent to a net N loss from N_2O emission alone of 64 $kg\,N\,ha^{-1}\,yr^{-1}$, was very high and exceeding previously reported fluxes from the Vejrumbro site (1.5–2.1 $g\,N_2O\,m^{-2}\,yr^{-1}$) (Nielsen et al., 2024) and German organic soils (0.04–6.3 $g\,N_2O\,m^{-2}\,yr^{-1}$ for grassland and cropland land uses) (Tiemeyer et al., 2020). The high N_2O emission from the transect during the measurement period indicate that N_2O may in fact dominate the GHG budget in relation to the global warming potential at this specific location at the Vejrumbro site had gross primary production (reducing net ecosystem CO_2 emission) been included in the measurements. It is important to reiterate here that the flux measurements of this study were done on bare soil whereas the studies referenced above included vegetation.

The high N_2O fluxes may be a result of high rates of denitrification in the subsoil from either *in situ* produced NO_3^- from peat decomposition or as NO_3-enriched agricultural runoff from the surrounding intensively cultivated areas, which was not affecting groundwater NO_3^- concentration in the center of the wetland with lower N_2O (Nielsen et al., 2024). The groundwater enters the northern peripheral zone of the wetland at Vejrumbro coinciding with the position of the measurement transect. The highest NO_3^- concentrations in groundwater at the SkyLine2D transect corresponded roughly with highest N_2O emissions during summer and early autumn (Figs. 7D–F and 8C), but the frequency of water sampling was too low to fully link groundwater NO_3^- temporal dynamics to N_2O emissions.

3.7.2 Temporal variability of net soil CO_2, CH_4 and N_2O fluxes

Time series of raw data of net soil CO_2, CH_4 and N_2O fluxes

With the high frequency of GHG flux measurements (on average 5 measurements per day per collar) it was possible to observe short term flux phenomena that in most studies deploying manual chambers are missed or if captured can lead to biased conclusions on flux magnitudes. For example, in most of the measurement points, CH_4 fluxes were generally near zero, but occasionally displayed elevated net emission for short periods even in periods with deeper WTD (Fig. 9A) for most chambers (see Fig. S5). This flux dynamic might be related to episodic release of accumulated CH_4 from deeper soil layers that are not fully oxidized in the aerated root zone and that were not released through plants (Askaer et al., 2011). As plants were not included in the collars these bursts cannot be attributed to plant emission pathways.

Generally, it was observed that soil CO_2 fluxes increased over the season with increasing temperature. However, some collars displayed rapid bursts of CO_2 emissions (example in Fig. 9A), while other collars at the same period did not display this behaviour (Fig. 9B). This dynamic points to different emission pathways from the soil not related to plant mediated transport. Thus, while we purposely omitted aboveground autotrophic respiration by clipping the vegetation, it cannot be ruled out that living roots inhabited the soil below the chambers and hence contributed to the observed CO_2 emission rates.

For N_2O, the spatiotemporal pattern was even more pronounced than for CO_2, with N_2O primarily emitted in bursts related to rapidly increasing or decreasing WTD that coincided with precipitation events. In drier periods with deeper WTD and little fluctuations, N_2O fluxes quickly dropped to near zero (Fig. 9A and B). Despite N_2O being emitted in similar temporal patterns across the transect, the magnitude of the N_2O peaks were not similar across the transect (Figs. 2, 8 and S5). Hence, the majority of N_2O is emitted in hot moments is likely driven by fluctuations in WTD (Fig. 9) as it has also been shown in other drained temperate peatland soils (Anthony and Silver, 2023).

Diurnal variation of net soil CO_2, CH_4 and N_2O fluxes

With the SkyLine2D system we observed a clear diurnal cycle for CO_2 and N_2O fluxes, but not for CH_4 (Fig. 10A–C). The lack of diurnal variability of CH_4 fluxes could also be due the removal of plants from the collars that would have facilitated light-driven fluxes (Askaer et al. 2011). The amplitude of diurnal variability increased with higher air temperature for CO_2 (Fig. 10B) and partly for N_2O (Fig. 10C). The month of July was an exception as it resembled the pattern observed in May although the July soil temperature was about 5 °C higher (Table 2). The lower N_2O fluxes observed
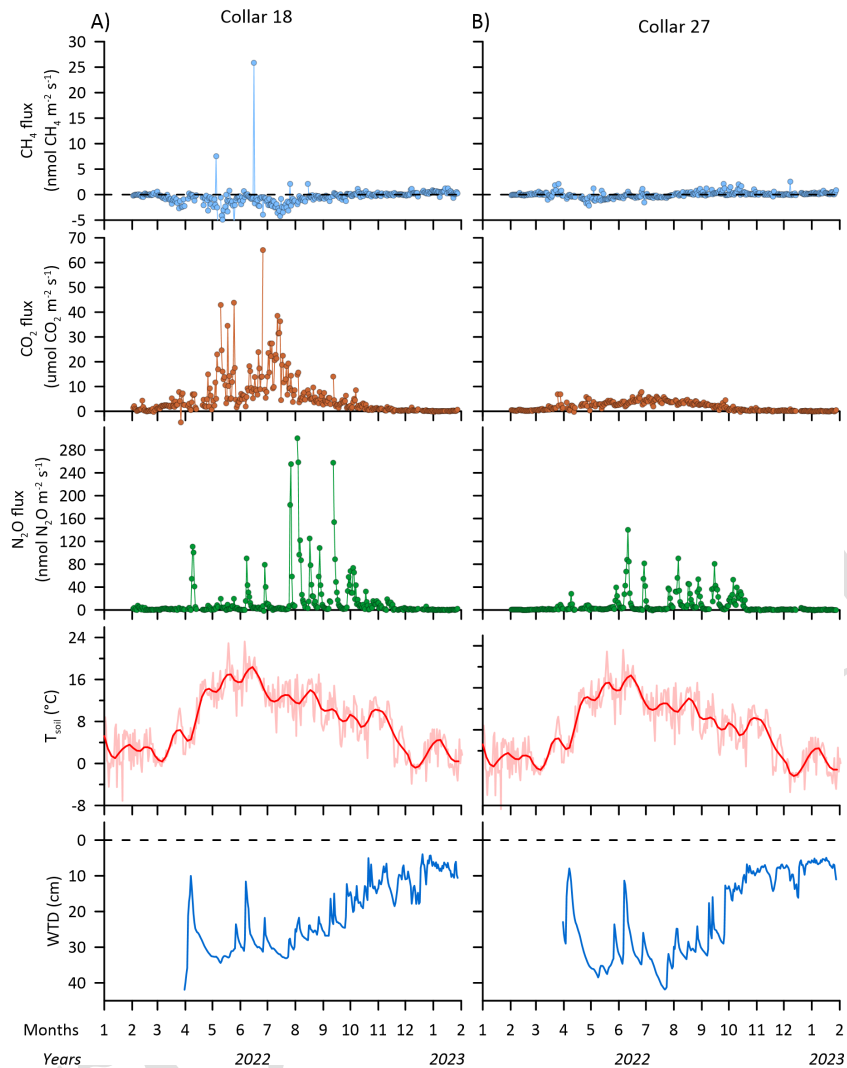
Figure 9. Examples of dai 〔average time series of CH_4, CO_2 and N_2O fluxes for collars 18 and 27 at the SkyLine2D transect in Vejrumbro, soil temperature (T_{soil}) [TS2] in celsius (°C) and groundwater table depth (WTD) in cm below terrain is shown in two lower panels for the measurement period from February 2022 to January 2023.

in July can be attributed to lower and more constant WTD in July compared to May, June and September across the transect (Fig. 5). Diurnal variability of soil CO_2 fluxes are well known and can be related to both increased heterotrophic respiration during the warmer day and autotrophic respiration in response to photosynthesis. Previously, similar diurnal patterns of N_2O emissions were observed in a Danish fen (Jørgensen et al., 2012).

Monthly variability of net soil GHG fluxes

The average soil GHG fluxes for all collars were summed to monthly transect sums to illustrate long term drivers on the flux magnitude. Overall, monthly sums of CO_2 and N_2O emissions increase with temperature and fluxes are highest under deeper WTD, but CH_4 net fluxes were less respon-

sive to long term changes in both temperature and hydrology (Fig. 11A–C). Net uptake of CH_4 increased slightly with increasing temperature and lower WTD during the spring and summer. With increasing water table and high temperatures in August the soils across the transect turned into a small net CH_4 source continuing in fall and winter (Fig. 11A).

For CO_2 the seasonal variation was pronounced and closely followed soil temperature until peak values in July for both transect average, minimum and maximum fluxes, respectively (Fig. 11B). From July to August, it was observed that WTD across the transect began to increase again and CO_2 fluxes departed from the close relation to soil temperature, indicating an inhibitory role of the WTD in this period, but reaching minimum fluxes in December, corresponding to the wettest and coldest month (Fig. 11B).
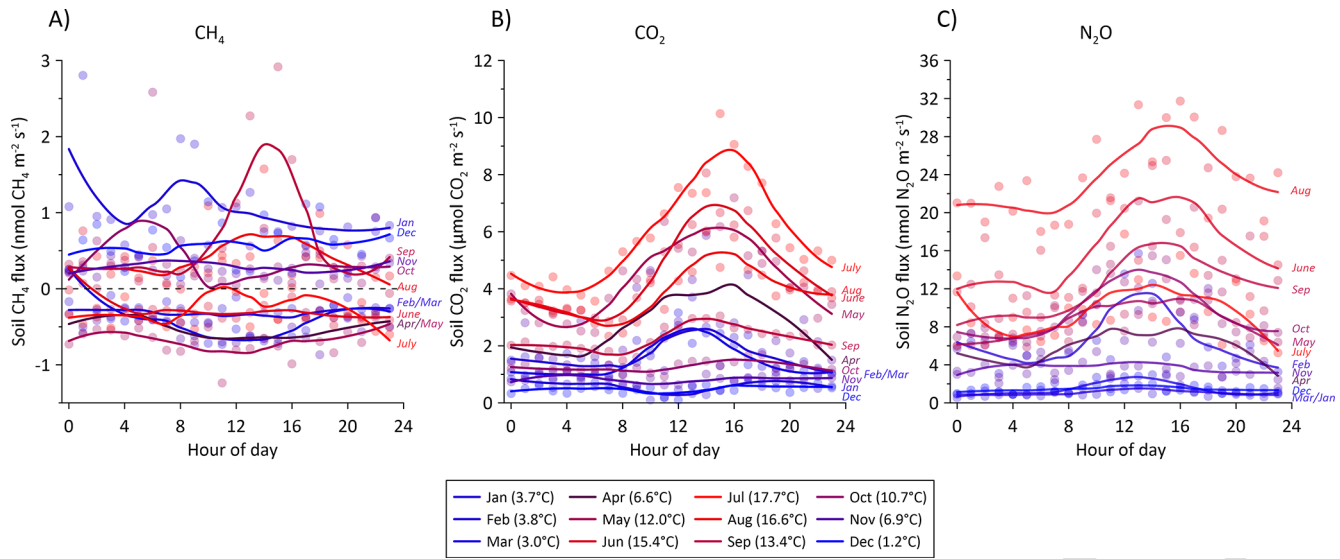
Figure 10. Average hourly flux for all soil collars of **(A)** CH_4, **(B)** CO_2, and **(C)** N_2O during a 24 h period. The diurnal variation is split between each month during the 2022–2023 measurement period. The fluxes were assigned the hour of measurement during the day and averaged per month. Color shade between blue and red corresponds to average air temperature for the specific month shown in parenthesis in the figure legend. Solid lines are loess fits for visualization of the diurnal variation in each month.
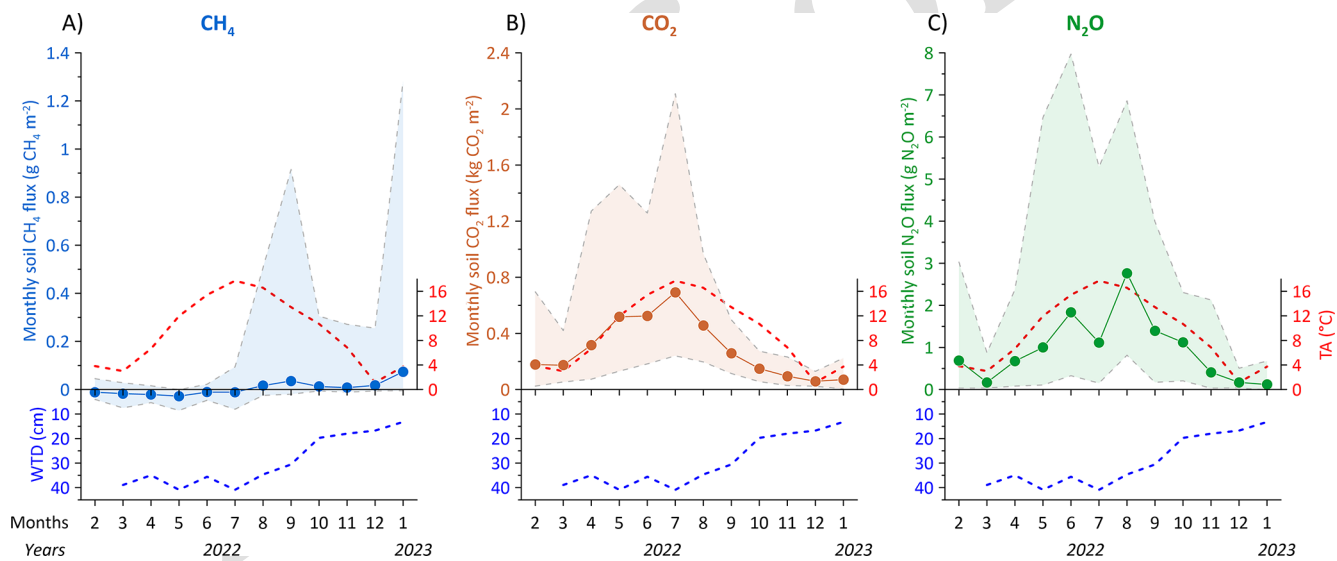
Figure 11. Monthly summed soil fluxes of **(A)** CH_4 in $g\,CH_4\,m^{-2}$, **(B)** CO_2 in $kg\,CO_2\,m^{-2}$, and **(C)** N_2O in $g\,N_2O\,m^{-2}$ for all organic soil collars for the measurement period from February 2022 to January 2023. Shaded areas for CH_4, CO_2 and N_2O graphs represent the maximum and minimum monthly average fluxes. Blue dashed line below CH_4, CO_2 and N_2O represent the measured monthly average transect groundwater table depth (WTD) in cm below terrain. Red dashed line shows the monthly average air temperature (TA).

Similarly, N_2O fluxes increased with soil temperature reaching peak monthly values in August, corresponding to the period of the year with highest soil temperature and increasing WTD (Fig. 11C). This supports the promoting role of soil water saturation on the production of N_2O when temperature is favourable for denitrification. N_2O fluxes reached minimum values in December when WTD and ST were lowest (Fig. 11C).

3.7.3 Ditch CO_2, CH_4 and N_2O fluxes

Time series of raw data of ditch CO_2, CH_4 and N_2O fluxes

Common for all three gases is that ditch emissions are dynamic and net fluxes change from zero to large net positive or negative fluxes within hours or days (Fig. 12A–C). Compared to net soil CH_4 fluxes the ditch can be considered

an emission hotspot at the Vejrumbro site (sum of diffusion and ebullition: $8.3\,\mathrm{g\,CH_4\,m^{-2}\,yr^{-1}}$), but fluxes are lower than earlier reports for ditches in other drained wetlands (between $0.1–44.3\,\mathrm{g\,CH_4\,m^{-2}\,yr^{-1}}$) (Peacock et al., 2021). Methane varies most throughout the measurement period with maximum diffusive flux close to $700\,\mathrm{nmol\,CH_4\,m^{-2}\,s^{-1}}$ and there was a tendency toward consistently higher net CH_4 emission from August to September, becoming close to zero in colder seasons (Fig. 12A). Ebullition of CH_4 did occur occasionally in the ditch, e.g. about 19.3 % of flux measurements for the ditch was comprised of ebullitions but constituted on average only 2.9 % of the total CH_4 emission ($0.24\,\mathrm{g\,CH_4\,m^{-2}\,yr^{-1}}$) from the ditch which is lower, but in the same range as a recent estimate from a ditch in a similar drained German peatland (Köhn et al., 2021). According to the flux calculation methodology, flux separation and extrapolation to daily sums, diffusive fluxes dominated ($6.56\,\mathrm{g\,CH_4\,m^{-2}\,yr^{-1}}$). However, it cannot be ruled out that the classification as diffusive flux may in fact be ebullition by nature. It has been suggested that microbubbles resulting from mass transport can resemble diffusive fluxes in a chamber making it difficult, if not impossible, to fully separate the two emission mechanisms in a continuous time series if headspace CH_4 concentrations do not abruptly increase (Prairie and del Giorgio, 2013), such as in the example shown in Fig. S4.

For CO_2, there was a general tendency towards lower fluxes during the summer months and fluxes increased in magnitude and variability towards the end of the study period (Fig. 12B). For N_2O, the fluxes fluctuated around zero for most of the study period, except towards the end (December and January) where net fluxes became positive (Fig. 12C). Compared to the net soil N_2O and CO_2 fluxes the ditch fluxes of these gases are low showing that the ditch is not contributing significantly to the CO_2 and N_2O budget at the Vejrumbro site.

Per square meter, the ditch emitted less N_2O ($0.41\,\mathrm{g\,N_2O\,m^{-2}}$ or $2.6\,\mathrm{kg\,N_2O\text{-}N\,ha^{-1}\,yr^{-1}}$) and CO_2 ($961\,\mathrm{g\,CO_2\,m^{-2}\,yr^{-1}}$ or $2.6\,\mathrm{t\,CO_2\text{-}C\,ha^{-1}\,yr^{-1}}$) than the organic soil, but was a hotspot of CH_4 emission ($8.4\,\mathrm{g\,CH_4\,m^{-2}\,yr^{-1}}$ or $63\,\mathrm{kg\,CH_4\text{-}C\,ha^{-1}\,yr^{-1}}$) during the measurement period. Although these emissions estimates are lower than previously reported for ditches in organic soil (up to $44\,\mathrm{g\,CH_4\,m^{-2}\,yr^{-1}}$) (Peacock et al., 2021). For the ditch CH_4 budget, ebullition only constitutes 2.9 % of net CH_4 emissions during the study period. This proportion may be underestimated as the count of ebullition events may have been underestimated (Prairie and del Giorgio, 2013).

Diurnal variability in ditch fluxes

For CH_4 fluxes, both diffusion and ebullition, there was no clear diurnal variability in any month (Fig. 13A and B). This is expected for ebullition emissions which is known to be erratic without any clear diurnality (Sø et al., 2023; Wik et al., 2016). For net CO_2 fluxes from the ditch there was no diurnal variability in colder seasons (January, February, March, November and December), but consistent positive net CO_2 efflux (Fig. 13C). Diurnal patterns became clearer with higher temperatures from May to October (Fig. 13C) and in this period CO_2 fluxes decreased during the day to sometimes reach net negative fluxes (net uptake of CO_2) during and after midday (Fig. 13C), although the net emissions were also observed in the daytime period (Fig. 13C). The net negative fluxes can likely be explained by photosynthetic activity of aquatic plants on the surface of the ditch or by algae in the water column which was measured due to the transparency of the chamber. Using an opaque chamber instead would likely have resulted in different net CO_2 efflux in daytime. For N_2O, the same pattern as for CH_4 was observed, where flux magnitude across the day fluctuated around zero, except for January where N_2O fluxes were consistently above zero (Fig. 13D).

Monthly variability in ditch fluxes

The monthly sums of CH_4 tend to increase with air temperature, although peak CH_4 emissions (September) occurred after air temperature peak (July) (Fig. 14A). Diffusive fluxes comprised the major emission pathway of CH_4 in the ditch (between 21 %–99 %), with the contribution from ebullition being highest in March (55 %) and April (78 %) (Fig. 14A). Water temperature in the ditch was relatively stable throughout the year, varying between $5.8–10.1\,°C$ being highest from April to November and lowest from December to March. However, there is little indication of a direct relation between ditch water temperature and net GHG fluxes (Fig. 14A–C).

For CO_2 and N_2O, the seasonal pattern is reversed with lowest fluxes during the warmest periods, approaching net zero or even net negative fluxes (Fig. 14B and C).

4 Data availability

Data for this publication is available for download via https://doi.org/10.60612/DATADK/BZQ8JE (Skov Nielsen et al., 2025).

5 Conclusion

The dataset presented here is unique for temperate fens and demonstrates the advantage of using automated GHG measurement systems to resolve temporal and spatial patterns of GHG dynamics in high detail. It represents a full year of data from 2022–2023 and must be considered specific to this period and the location at Vejrumbro. Consequently, it is expected that the annual budget of all GHGs in other years will likely differ due to varying climatic and hydrological conditions.

Specifically, the dataset demonstrates how temporal variation in soil hydrology and temperature is linked to the tem-
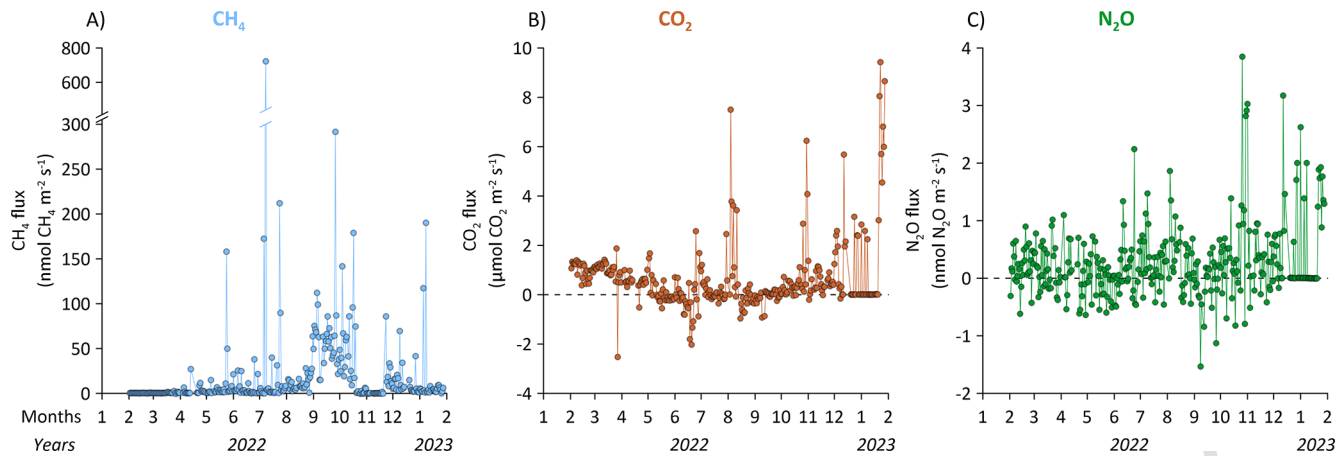
Figure 12. Daily average time series of net ditch total **(A)** CH_4 (diffusion and ebullition), **(B)** CO_2, and **(C)** N_2O fluxes at the Vejrumbro site for the measurement period from February 2022 to January 2023.
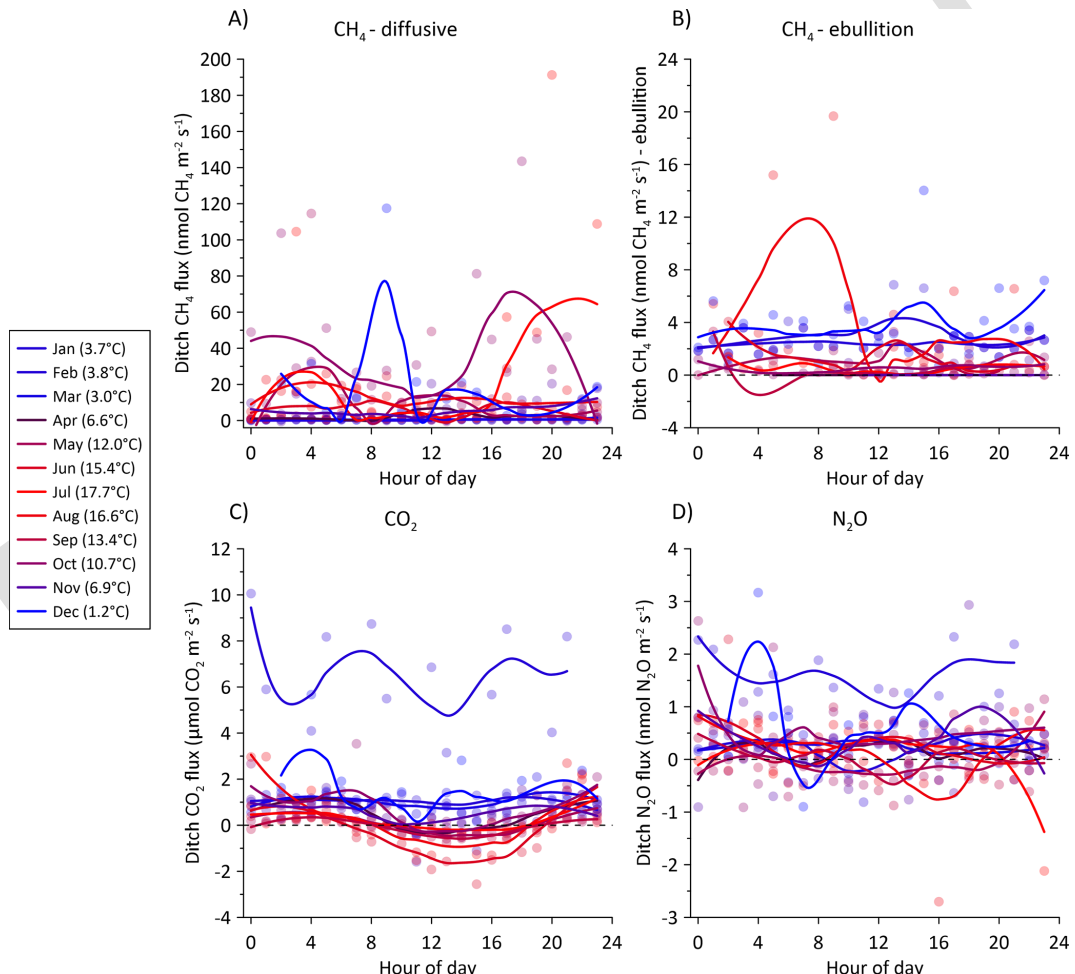
Figure 13. Average hourly fluxes for the ditch collar of **(A)** diffusive CH_4 fluxes, **(B)** CH_4 ebullition fluxes, **(C)** CO_2, and **(D)** N_2O during a 24 h period. The fluxes were assigned the hour of measurement during the day and averaged per month. The diurnal variation is split between each month during the 2022–2023 measurement period. Color shade between blue and red corresponds to average air temperature for the specific month shown in parenthesis in the figure legend. Solid lines are loess fits for visualization of the diurnal variation in each month. Note different axes.
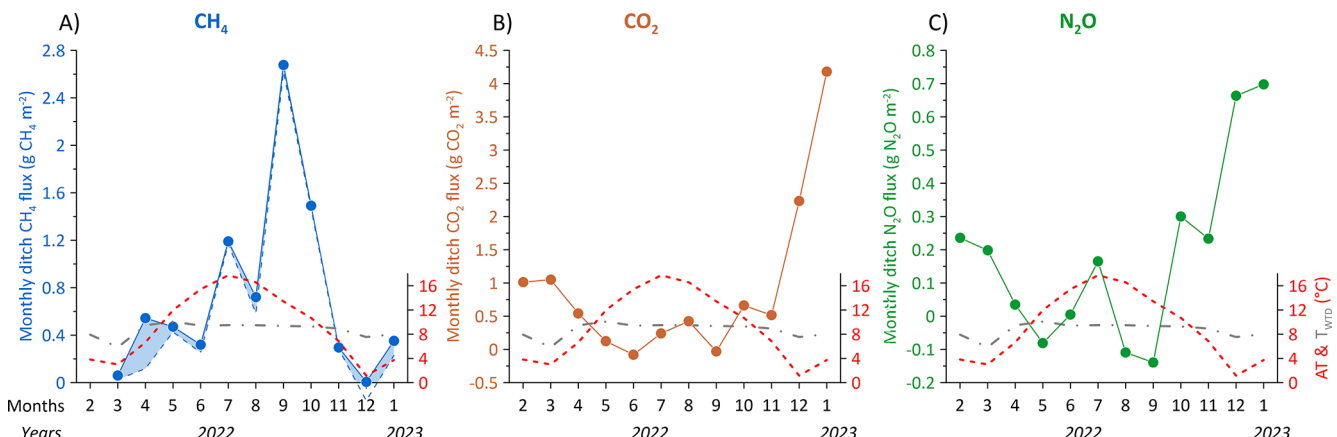
Figure 14. Monthly summed ditch fluxes of **(A)** CH_4 in $g\,CH_4\,m^{-2}$, **(B)** CO_2 in $g\,CO_2\,m^{-2}$ and **(C)** N_2O in $g\,N_2O\,m^{-2}$ for the measurement period from February 2022 to January 2023. In **(A)** the blue dashed line is the contribution of diffusive fluxes and the shaded blue area between the full and dashed blue lines represent the monthly contribution of ebullition to the total flux. Red and grey dashed lines show the monthly average air (AT) and groundwater temperature (T_{WTD}) in °C, respectively.

poral variation of fluxes. Interestingly, the temporal variability of GHG fluxes across the transect appears to be lower than the spatial variation highlighting that spatial variability in hydrology and temperature may not necessarily be the best predictor of flux magnitudes across the transect. The cause of spatial variability in GHG fluxes remains unresolved and does not clearly link directly to either water table depth (WTD), soil temperature, or soil/groundwater chemical parameters.

The initial harvest and herbicide application represent ecosystem disturbances that could potentially alter soil biogeochemistry. However, these were conducted months prior to the start of flux measurements, minimizing the direct effect of herbicide. Continued plant removal from inside the collars was necessary for flux measurements, meaning the fluxes may only be regarded as net soil GHG fluxes and not representative of net ecosystem exchange. Excluding vegetation likely influenced measured fluxes of soil respiration (e.g., excluding root exudates) and reduced plant-mediated CH_4 and N_2O emissions, potentially also reducing interannual variability.

– *Carbon dioxide fluxes*. The magnitude of annual cumulative CO_2 fluxes is in the same range as other studies of temperate fens. Temporal variability is largely governed by the seasonality of WTD and soil temperature (T_{soil}). TS3 Soil CO_2 fluxes showed diurnal variability with higher fluxes during midday, where the amplitude between night and day was augmented with T_{soil}. TS4

– *Nitrous oxide fluxes*. Cumulative soil N_2O fluxes exceed previously reported values for temperate fens at the Vejrumbro site and others. Unlike CO_2, N_2O is emitted largely in pulses related to rapid fluctuations of WTD, which increase in size with T_{soil}, TS5 indicating a seasonal regulation of N_2O production by temperature.

These measurements suggest an important but difficult-to-capture dynamic of N_2O in peatlands, where hot moments during warm periods determine most of the annual emissions. Soil N_2O fluxes also showed diurnal variability similar to CO_2.

– *Methane fluxes*. The peat soils across the transect were insignificant sources of CH_4 during the measurement period. This could be linked to deeper WTD (20–40 cm) during summer, a cold wet winter, and the presence of alternative electron acceptors (NO_3^-, SO_4^{2-}, and Fe^{3+}), which provide suboptimal conditions for CH_4 production. Vegetation removal may have further impeded CH_4 emissions by restricting plant-mediated pathways. Soil CH_4 fluxes did not show diurnal variability.

The ditch at the transect was a net source of both N_2O and CO_2, but at magnitudes 27 and 4 times lower than the soil GHG fluxes, respectively. It acted as a CH_4 source, comparable to other ditches in temperate fens. CH_4 was emitted mostly through diffusive emissions from the water surface, with occasional observations of ebullition.

This dataset provides a unique opportunity to test hypotheses regarding spatial and temporal patterns of GHG emissions and their drivers in peatlands. It supports the development of models that predict soil GHG fluxes in response to soil temperature and hydrology (WTD), aiding in the prediction of reliable budgets for locations beyond Vejrumbro. We intend to publish this dataset to the research community so that experimentalists and modelers can use it to explore basic hydrological and thermal regulation of GHG fluxes and develop predictive models for spatiotemporal variability.

Supplement. The supplement related to this article is available online at [the link will be implemented upon publication].

References

Anthony, T. L. and Silver, W. L.: Hot spots and hot moments of greenhouse gas emissions in agricultural peatlands, Biogeochemistry, 167, 461–477, https://doi.org/10.1007/s10533-023-01095-y, 2023.

Askaer, L., Elberling, B., Friborg, T., Jørgensen, C. J., and Hansen, B. U.: Plant-mediated CH_4 transport and C gas dynamics quantified in-situ in a Phalaris arundinacea-dominant wetland, Plant Soil, 343, 287–301, https://doi.org/10.1007/s11104-011-0718-x, 2011.

Boonman, J., Buzacott, A. J. V, van den Berg, M., van Huissteden, C., and van der Velde, Y.: Transparent automated CO_2 flux chambers reveal spatial and temporal patterns of net carbon fluxes from managed peatlands, Ecol. Indic., 164, 112121, https://doi.org/10.1016/j.ecolind.2024.112121, 2024.

Bridgham, S. D., Cadillo-Quiroz, H., Keller, J. K., and Zhuang, Q.: Methane emissions from wetlands: biogeochemical, microbial, and modeling perspectives from local to global scales, Glob. Chang. Biol., 19, 1325–1346, https://doi.org/10.1111/gcb.12131, 2013.

Christiansen, J. R., Outhwaite, J., and Smukler, S. M.: Comparison of CO_2, CH_4 and N_2O soil-atmosphere exchange measured in static chambers with cavity ring-down spectroscopy and gas chromatography, Agric. For. Meteorol., 211–212, 48–57, https://doi.org/10.1016/j.agrformet.2015.06.004, 2015.

Christiansen, J. R., Levy-Booth, D., Prescott, C. E., and Grayston, S. J.: Microbial and Environmental Controls of Methane Fluxes Along a Soil Moisture Gradient in a Pacific Coastal Temperate Rainforest, Ecosystems, 19, 1255–1270, https://doi.org/10.1007/s10021-016-0003-1, 2016.

Evans, C. D., Peacock, M., Baird, A. J., Artz, R. R. E., Burden, A., Callaghan, N., Chapman, P. J., Cooper, H. M., Coyle, M., Craig, E., Cumming, A., Dixon, S., Gauci, V., Grayson, R. P., Helfter, C., Heppell, C. M., Holden, J., Jones, D. L., Kaduk, J., Levy, P., Matthews, R., McNamara, N. P., Misselbrook, T., Oakley, S., Page, S. E., Rayment, M., Ridley, L. M., Stanley, K. M., Williamson, J. L., Worrall, F., and Morrison, R.: Overriding water table control on managed peatland greenhouse gas emissions, Nature, 593, 548–552, https://doi.org/10.1038/s41586-021-03523-1, 2021.

Jørgensen, C. J., Struwe, S., and Elberling, B.: Temporal trends in N_2O flux dynamics in a Danish wetland – effects of plant-mediated gas transport of N_2O and O_2 following changes in water level and soil mineral-N availability, Glob. Chang. Biol., 18, 210–222, https://doi.org/10.1111/j.1365-2486.2011.02485.x, 2012.

Jørgensen, M. S., Plauborg, F., and Kørup, K.: Climate normal for Foulum 1991–2020, Aarhus University, https://dcapub.au.dk/djfpublikation/djfpdf/DCArapport223.pdf (last access: 24 November 2025), 2023.

Kandel, T. P., Lærke, P. E., and Elsgaard, L.: Annual emissions of CO_2, CH_4 and N_2O from a temperate peat bog: Comparison of an undrained and four drained sites under permanent grass and arable crop rotations with cereals and potato, Agric. For. Meteorol., 256–257, 470–481, https://doi.org/10.1016/j.agrformet.2018.03.021, 2018.

Koch, J., Elsgaard, L., Greve, M. H., Gyldenkærne, S., Hermansen, C., Levin, G., Wu, S., and Stisen, S.: Water-table-driven greenhouse gas emission estimates guide peatland restoration at national scale, Biogeosciences, 20, 2387–2403, https://doi.org/10.5194/bg-20-2387-2023, 2023.

Köhn, D., Welpelo, C., Günther, A., and Jurasinski, G.: Drainage Ditches Contribute Considerably to the CH_4 Budget of a Drained and a Rewetted Temperate Fen, Wetlands, 41, 71, https://doi.org/10.1007/s13157-021-01465-y, 2021.

Nguyen, D. B., Rose, M. T., Rose, T. J., Morris, S. G., and van Zwieten, L.: Impact of glyphosate on soil microbial biomass and respiration: A meta-analysis, Soil Biol. Biochem., 92, 50–57, https://doi.org/10.1016/j.soilbio.2015.09.014, 2016.

Nielsen, C. K., Liu, W., Koppelgaard, M., and Laerke, P. E.: To Harvest or not to Harvest: Management Intensity did not Affect Greenhouse Gas Balances of Phalaris Arundinacea Paludiculture, Wetlands, 44, 79, https://doi.org/10.1007/s13157-024-01830-7, 2024.

Padilla, J. T. and Selim, H. M.: Environmental behavior of glyphosate in soils, Advances in Agronomy, 159, 1–34, https://doi.org/10.1016/BS.AGRON.2019.07.005, 2020.

Peacock, M., Audet, J., Bastviken, D., Cook, S., Evans, C. D., Grinham, A., Holgerson, M. A., Högbom, L., Pickard,

A. E., Zieliński, P., and Futter, M. N.: Small artificial waterbodies are widespread and persistent emitters of methane and carbon dioxide, Glob. Chang. Biol., 27, 5109–5123, https://doi.org/10.1111/gcb.15762, 2021.

Pihlatie, M. K., Christiansen, J. R., Aaltonen, H., Korhonen, J. F. J., Nordbo, A., Rasilo, T., Benanti, G., Giebels, M., Helmy, M., Sheehy, J., Jones, S., Juszczak, R., Klefoth, R., Lobo-do-Vale, R., Rosa, A. P., Schreiber, P., Serça, D., Vicca, S., Wolf, B., and Pumpanen, J.: Comparison of static chambers to measure CH_4 emissions from soils, Agric. For. Meteorol., 171–172, 124–136, https://doi.org/10.1016/j.agrformet.2012.11.008, 2013.

Prairie, Y. T. and del Giorgio, P. A.: A new pathway of freshwater methane emissions and the putative importance of microbubbles, Inland Waters, 3, 311–320, https://doi.org/10.5268/IW-3.3.542, 2013.

Reza Mashhadi, S., Grombacher, D., Zak, D., Erik Lærke, P., Estrup Andersen, H., Christian Hoffmann, C., and Jes Petersen, R.: Borehole nuclear magnetic resonance as a promising 3D mapping tool in peatland studies, Geoderma, 443, 116814, https://doi.org/10.1016/j.geoderma.2024.116814, 2024.

Rheault, K., Christiansen, J. R., and Larsen, K. S.: goFlux: A user-friendly way to calculate GHG fluxes yourself, regardless of user experience, J. Open Source Softw., 9, 6393, https://doi.org/10.21105/joss.06393, 2024.

Skov Nielsen, A., Steenberg Larsen, K., Lærke, P. E., Rodriguez, A. F., Pullens, J. W. M., Petersen, R. J., and Christiansen, J. R.: Supporting Data for: A full year of continuous net soil and ditch CO_2, CH_4, N_2O fluxes, soil hydrology and meteorology for a drained fen in Denmark, DeiC [data set], https://doi.org/10.60612/DATADK/BZQ8JE, 2025.

Sø, J. S., Sand-Jensen, K., Martinsen, K. T., Polauke, E., Kjær, J. E., Reitzel, K., and Kragh, T.: Methane and carbon dioxide fluxes at high spatiotemporal resolution from a small temperate lake, Science of The Total Environment, 878, 162895, https://doi.org/10.1016/j.scitotenv.2023.162895, 2023.

Tiemeyer, B., Freibauer, A., Borraz, E. A., Augustin, J., Bechtold, M., Beetz, S., Beyer, C., Ebli, M., Eickenscheidt, T., Fiedler, S., Förster, C., Gensior, A., Giebels, M., Glatzel, S., Heinichen, J., Hoffmann, M., Höper, H., Jurasinski, G., Laggner, A., Leiber-Sauheitl, K., Peichl-Brak, M., and Drösler, M.: A new methodology for organic soils in national greenhouse gas inventories: Data synthesis, derivation and application, Ecol. Indic., 109, 105838, https://doi.org/10.1016/j.ecolind.2019.105838, 2020.

Vroom, R. J. E., van den Berg, M., Pangala, S. R., van der Scheer, O. E., and Sorrell, B. K.: Physiological processes affecting methane transport by wetland vegetation – A review, Aquat. Bot., 182, 103547, https://doi.org/10.1016/j.aquabot.2022.103547, 2022.

Wik, M., Varner, R. K., Anthony, K. W., MacIntyre, S., and Bastviken, D.: Climate-sensitive northern lakes and ponds are critical components of methane release, Nat. Geosci., 9, 99–105, https://doi.org/10.1038/ngeo2578, 2016.

Remarks from the typesetter

TS1   You mentioned here that the "depth value is missing". The correct value was not found in the proofreading files. Please provide the correct value as well as a short explanation regarding the missing information that can be forwarded by us to the editor to ask for approval.

TS2   Should this be ST?

TS3   The comment here read "Seems odd to change the abbreviation of soil temperature from ST to Tsoil here in the conclusion." There was another instance of Tsoil in the article which has now been highlighted. Should these be change to ST?

TS4   Should this be ST?

TS5   Should this be ST?